

1 **How much is particulate matter near the ground influenced**
2 **by upper level processes within and above the PBL? A**
3 **summertime case study in Milan (Italy) evidences the**
4 **distinctive role of nitrate**

5

6 **G. Curci¹, L. Ferrero², P. Tuccella¹, F. Barnaba³, F. Angelini⁴, E. Bolzacchini², C.**
7 **Carbone⁵, H. A. C. Denier van der Gon⁶, M. C. Facchini⁵, G. P. Gobbi³, J. P. P.**
8 **Kuenen⁶, T. C. Landi⁵, C. Perrino⁷, M. G. Perrone², G. Sangiorgi² and P. Stocchi⁵**

9 [1]{CETEMPS Centre of Excellence, Dept. Physical and Chemical Sciences, Univ. L'Aquila, L'Aquila, Italy}

10 [2]{POLARIS Research Centre, Dept. of Earth and Environmental Sciences, Univ. Milano Bicocca, Milano,
11 Italy}

12 [3]{Institute for Atmospheric and Climate Sciences (ISAC), National Research Council (CNR), Rome, Italy}

13 [4]{Italian National agency for new technologies, Energy and sustainable economic development (ENEA),
14 Rome, Italy}

15 [5]{Institute for Atmospheric and Climate Sciences (ISAC), National Research Council (CNR), Bologna, Italy}

16 [6] {TNO Climate, Air and Sustainability, Princetonlaan 6, 3584 CB Utrecht, The Netherlands}

17 [7]{Institute of Atmospheric Pollution Research (IIA), National Research Council (CNR), Rome, Italy}

18 Correspondence to: Gabriele Curci (gabriele.curci@aquila.infn.it)

19

20

1 **Abstract**

2 Chemical and dynamical processes lead to the formation of aerosol layers in the upper
3 planetary boundary layer (PBL) and above it. Through vertical mixing and entrainment into
4 the PBL these layers may contribute to the ground-level particulate matter (PM), however to
5 date a quantitative assessment of such a contribution has not been carried out. This study
6 investigates this aspect by combining chemical and physical aerosol measurements with
7 WRF/Chem model simulations. The observations were collected in the Milan urban area
8 (Northern Italy) during summer of 2007. The period coincided with the passage of a
9 meteorological perturbation that cleansed the lower atmosphere, followed by a high pressure
10 period favouring pollutant accumulation. Lidar observations revealed the formation of
11 elevated aerosol layers and evidence of their entrainment into the PBL. We analyzed the
12 budget of ground-level PM_{2.5} (particulate matter with an aerodynamic diameter less than 2.5
13 μm) with the help of the online meteorology-chemistry WRF/Chem model, focusing in
14 particular on the contribution of upper level processes. Our findings show that an important
15 player in determining the upper PBL aerosol layer is particulate nitrate, which may reach
16 higher values in the upper PBL (up to 30% of the aerosol mass) than in the lower PBL. The
17 nitrate formation process is predicted to be largely driven by the relative humidity vertical
18 profile, which may trigger efficient aqueous nitrate formation when exceeding the ammonium
19 nitrate deliquescence point. Secondary PM_{2.5} produced in the upper half of the PBL may
20 contribute up to 7-8 μg/m³ (or 25%) to ground level concentrations on an hourly basis. A
21 large potential role is also found to be played by the residual aerosol layer above the PBL,
22 which may occasionally contribute up to 10-12 μg/m³ (or 40%) to hourly ground level PM_{2.5}
23 concentrations during the morning hours. Although the results presented here refer to one
24 relatively short period in one location, this study highlights the importance of considering the
25 interplay between chemical and dynamical processes occurring within and above the PBL
26 when interpreting ground level aerosol observations.

27

1 **1 Introduction**

2 The understanding of processes governing atmospheric aerosols is primarily motivated by
3 their adverse effects on health and their contribution to the radiative budget of the
4 atmosphere. Diseases affecting the respiratory system have been linked to inhalation of
5 aerosols, especially their finer and more numerous fraction (Beelen et al., 2014; Oberdorster,
6 2001), although the mechanisms underlying the health effect associated to size, number and
7 composition of particulate matter have only recently begun to be disclosed (Harrison and Yin,
8 2000; Daher et al., 2012; Perrone et al., 2013). Aerosols affect the atmospheric energy balance
9 directly, by scattering and absorbing radiation (Yu et al., 2006), indirectly, by serving as
10 cloud condensation nuclei (Lohmann and Feichter, 2005), and semi-directly, by heating the
11 air through absorption of radiation and reducing low cloud cover (Johnson et al., 2004). The
12 assessment of these effects caused by aerosols is still characterized by large uncertainties,
13 since our knowledge of the processes determining their abundance, size distribution, and
14 chemical composition, which strongly vary in space and time, is still limited (Raes et al.,
15 2000; Poschl, 2005). Here we focus on the interplay between dynamical and chemical
16 processes in the vertical direction, in order to better understand the budget terms making up
17 the ground level particulate matter, a common measure to evaluate air quality. The study
18 focuses on the urban environment of Milan, situated in the center of Italy's Po Valley , a
19 European hot-spot for atmospheric pollution.

20 The correlation between pollutants at the surface and meteorological variables is well
21 established and the fundamental role played by the variables associated to the vertical mixing
22 in the planetary boundary layer (PBL) has been highlighted both for ozone (Di Carlo et al.,
23 2007, and references therein) and particulate matter (Tai et al., 2010, and references therein).
24 Moreover, Zhang and Rao (1999) analyzed aircraft and tower measurements over the Eastern
25 United States and showed that elevated nocturnal layers rich in ozone and its precursors aloft,
26 remnant of the previous day's mixed layer, may strongly affect ground-level ozone levels on
27 the following morning as vertical motions mix upper and surface air. The same authors
28 suggested that a reduction of ozone and precursors aloft may be more effective in reducing
29 pollution than local emission cuts, thus calling for a region-wide strategy for emissions
30 control. Aerosols are also known to form layers above or near the top of the mixing layer,
31 especially when stability and presence of clouds increase (e.g. O'Dowd and Smith, 1996).
32 Similarly to ozone, an aerosol residual layer aloft is often observed (e.g. Di Giuseppe et al.,

1 2012), which may influence the aerosol at the surface, as witnessed by similar size-
2 distributions (Maletto et al., 2003). A significant contribution to surface aerosol from
3 entrainment and vertical dilution and chemical net production in the boundary layer has also
4 been pointed out in recent studies using single-column models (van Stratum et al., 2012;
5 Ouwersloot et al., 2012).

6 The nontrivial relationship between ground- and upper-level aerosols burden is illustrated by
7 comparing of surface particulate matter (PM) mass concentrations to aerosol optical depth
8 (AOD), which is proportional to the aerosol column load (typically measured by ground-
9 based sun-photometers or retrieved from satellites). In a well mixed PBL, the AOD may
10 exhibit a high correlation with surface PM, especially with its fine fraction, and indeed this
11 assumption is often exploited to infer surface PM_{2.5} (PM with diameter < 2.5 μm) from
12 satellite AOD observations (e.g. van Donkelaar et al., 2010). However, that assumption does
13 not always hold true, due to the presence of significant aerosol stratification aloft, and
14 noticeable differences which may occur between AOD and surface PM behaviour may occur,
15 such as in the timing of daily peak values or in multi-day trends (Barnaba et al., 2007, 2010;
16 Boselli et al., 2009; Estelles et al., 2012; He et al., 2012). Analyzing two-year measurements
17 in the Po Valley (Italy), Barnaba et al. (2010) indeed pointed out that annual cycles of AOD
18 and surface PM₁₀ (PM with diameter < 10 μm) display a remarkable opposite phase. While
19 PM₁₀ peaks in winter, due to the reduced dilution by a shallower PBL and to the condensation
20 of semi-volatile species favoured by the lower temperatures, AOD peaks in summer, because
21 of a more persistent presence of an aerosol residual layer aloft, which contributes up to 30%
22 of the total AOD.

23 Aircraft measurements also showed intriguing features of aerosol vertical gradients in the
24 lower troposphere, in particular when looking at different chemical components. Several
25 studies reported a generally constant or slightly decreasing profile in the convective boundary
26 layer of sulfate and organic matter as opposed to an increasing profile of nitrate (Neuman et
27 al., 2003; Cook et al., 2007; Crosier et al., 2007; Morgan et al., 2009; Ferrero et al., 2012).
28 Neuman et al. (2003) attributed the enhanced nitrate layer near the top of the PBL to the lower
29 temperatures that favour gas-phase nitric acid (HNO₃) and ammonia (NH₃) conversion to
30 particulate ammonium nitrate. The same authors also pointed out that nitrate and HNO₃
31 display sharp vertical gradients in the PBL, as opposed to other directly emitted (carbon
32 monoxide) or secondary (ozone) species that are relatively uniform, and this observation was

1 interpreted as an indication that thermodynamic equilibrium between gas and particle phases
2 occurs faster than vertical mixing. However, the issue is still under debate as subsequent
3 model studies found that an instantaneous thermodynamic equilibrium between HNO₃ and
4 nitrate yields excessively steep and unrealistic vertical gradients (Morino et al., 2006; de
5 Brugh et al., 2012). Moreover, the presence of aerosol layers enriched with sulfate and water-
6 soluble carbonaceous matter was observed above the boundary layer or in convective clouds
7 during several aircraft campaigns over North America (Novakov et al., 1997; Heald et al.,
8 2006; Duong et al., 2011; Wonaschuetz et al., 2012), and attributed to biomass burning
9 plumes or aqueous-chemistry processes.

10 A quantitative assessment of the contribution of elevated aerosol layers and related dynamical
11 and chemical processes to ground-level particulate matter level is still lacking. Recent
12 modelling studies that reported budget (or process) analyses of the simulated aerosol mainly
13 focused on terms of the continuity equation at the surface or on integrated values over the
14 whole boundary layer. Surface and PBL total PM_{2.5} mass is calculated to be mainly produced
15 by direct emissions and secondary formation by aerosol processes (e.g. condensation and
16 absorption) and removed by horizontal and vertical transport and wet deposition (Zhang et al.,
17 2009; Liu et al., 2011). The controlling processes are different for surface PM number, which
18 is accumulated mainly by homogeneous nucleation and vertical transport and it is lost mainly
19 by dry deposition and coagulation (Zhang et al., 2010).

20 For primary components such as black carbon (BC) the fate is similar to that of total PM_{2.5},
21 while for secondary species it is more intricate. Sulfate is generally produced in the PBL by
22 aerosol and clouds processes (the latter being very important) and exported out of the PBL
23 throughout the year (de Meij et al., 2007; Zhang et al., 2009; de Brugh et al., 2011; Liu et al.,
24 2011). Averaged over the year, the nitrate budget is similar to that of sulfate, with the
25 difference that cloud processes (wet deposition) are a sink (de Brugh et al., 2011; Liu et al.,
26 2011). However, during the summer there might be competition between PM production (e.g.
27 condensation and absorption) and destruction (e.g. evaporation and desorption) processes, and
28 PBL may become a sink and not a source for nitrate (Zhang et al., 2009). The same
29 competition between PM production and destruction processes affect the secondary organic
30 aerosols (SOA) throughout the year (Zhang et al., 2009). Moreover, SOA are strongly
31 influenced by biogenic volatile organic compounds (BVOC) emissions, through semi-volatile

1 products of the isoprene and terpenes oxidation, which also have a marked seasonal cycle
2 (Zhang et al., 2007; Hodzic et al., 2009).

3 In the present study, we examined the formation of aerosol near the surface in the particular
4 perspective of the boundary layer vertical processes outlined above. We analyzed aerosol
5 mass observations, composition, number and optical properties in the month of July 2007 in
6 Milan (45°N, 9°E, Northern Italy) during the intensive campaigns carried within the
7 framework of the QUITSAT (“Air Quality by the Integration of Ground- and Satellite-based
8 Observations and Multiphase Chemistry-Transport Modelling”, funded by the Italian Space
9 Agency, ASI) and AeroClouds (“Study of Direct and Indirect Effect of Aerosols and Clouds
10 on Climate”, funded by the Italian Ministry for Higher Education) projects. The experimental
11 results were then complemented/interpreted through WRF/Chem model simulations.

12 Firstly, what is known about the aerosol phenomenology in the investigated domain is briefly
13 reviewed in section 2. We describe the experimental setup in section 3 and the model setup in
14 section 4. In section 5, a preliminary analysis of the observations is carried out in order to
15 characterize the relevant features of the case study and pose questions arising from the picture
16 given by the measurements. Then, these questions are addressed using WRF/Chem model
17 simulations. After a model validation against available observations, we analyze the budget of
18 aerosol species as calculated by the model, focusing in particular on the vertical dimension.
19 The main results are summarized in conclusive section 6.

20

21 **2 The investigated domain**

22 Milan is the largest urban area in Italy (c.a. 5 million people) and lies in one of the most
23 polluted areas of Europe, the Po Valley (Putaud et al., 2010). The topography of the valley
24 (closed by the Alps to the North and West, and by the Apennine to the South), under high-
25 pressure systems, favour stagnant atmospheric conditions and recirculation of air through the
26 typical mountain-valley breeze (Dosio et al., 2002). The local circulation in combination with
27 elevated anthropogenic emissions especially from traffic, residential combustion, and
28 agriculture (Lonati et al., 2005; Carnevale et al., 2008; Perrone et al., 2012; Saarikoski et al.,
29 2012) makes it a nitrogen dioxide and aerosol hot-spot clearly visible from space (e. g. Chu et
30 al., 2003; Barnaba and Gobbi, 2004; Ordóñez et al., 2006; van Donkelaar et al., 2010).

1 At the surface, PM₁₀ annual mean in Milan has been stable between 50 and 60 µg/m³ in the
2 last decade (Carnevale et al., 2008; Silibello et al., 2008), thus systematically above the
3 European limit of 40 µg/m³ for human protection (EC, 2008). The winter average values are
4 roughly double than those in the summer, and peak values are up to 200 µg/m³ (Marcazzan et
5 al., 2001). The main aerosol components are sulfate, nitrate, and organic matter (OM), which
6 account for roughly 20%, 15%, 40%, respectively, of PM₁₀ mass in summer, and 10%, 30%,
7 50%, respectively, in winter (Marcazzan et al., 2001; Putaud et al., 2002; Lonati et al., 2005;
8 Carbone et al., 2010; Perrone et al., 2010; Daher et al., 2012). These values are similar to
9 those in other urban areas in the Po Valley (Matta et al., 2003; Carbone et al., 2010; Squizzato
10 et al., 2013). Most of the mass of those species is distributed in the accumulation mode
11 (particle diameter in the range 0.14-1.2 µm), while the coarse mode (1.2-10 µm diameter) has
12 a larger fraction of crustal material and sea salts (Matta et al., 2003; Carbone et al., 2010). In
13 summer, nitrate can exhibit a broader size distribution as a larger fraction may also form in
14 the coarse mode. Higher temperatures, lower humidity, higher load of sulphate competing for
15 the uptake of ammonia, are less favourable to ammonium nitrate accumulation in the fine
16 mode. As a consequence, more nitric acid is available to react with soil dust or sea salt
17 leading to the formation of mineral nitrate on coarse particles. (Matta et al., 2003; Hodzic et
18 al., 2006; Lee et al., 2008 ; Carbone et al., 2010). The total number concentration of aerosol is
19 of the order of 10⁴ cm⁻³, with the ultrafine (diameter d < 100 nm) and submicron (100 < d <
20 1000 nm) particles constituting up to 80% and 20% of the total, respectively (Lonati et al.,
21 2011). The aerosol number concentration is usually distributed in three modes (Balternsperger
22 et al., 2002; Lonati et al., 2011). One mode with diameters in the range of 20-30 nm,
23 consisting of hydrophobic and highly volatile organic material originating from combustion
24 (Baltensperger et al., 2002), plus new particles from nucleation events that occur on about
25 35% of the days in Po Valley (Hamed et al., 2007). The other two modes are in the submicron
26 range (dry diameters 50-200 nm), one almost hydrophobic, related to primary emissions (e.g.
27 soot), and the other hydrophilic, related to secondary aerosols (Balternsperger et al., 2002).

28 The aerosol vertical profile in Milan and in the wider Po Valley region was characterized by
29 means of aircraft, Lidar, and tethered balloon measurements (Highwood et al. 2007; Barnaba
30 et al., 2007; Barnaba et al., 2010; Crosier et al., 2007; Angelini et al., 2009; Ferrero et al.,
31 2010; Ferrero et al., 2011). Similarly to other polluted valley areas, two layers with distinct
32 characteristics are often found. One in the PBL which is humid, rich in fresh emissions, with

1 the nitrate profile increasing with height, and another layer, above the PBL, with more aged
2 aerosols enriched in the sulfate and organic matter fraction (Highwood et al., 2007; Crosier et
3 al., 2007; Ferrero et al., 2010). This decoupling into two layers is attributed to the mountain-
4 valley breeze dynamics (Angelini et al., 2009) and to the sporadic arrival of long-range
5 transported Saharan dust (Barnaba et al., 2007) or biomass burning plumes (Barnaba et al.,
6 2011). The number concentration of fine mode ($d < 1.6 \mu\text{m}$) particles are found to be
7 relatively constant with height in the PBL, and it decreases by a factor of 2-3 above the PBL.
8 In contrast, coarse particle ($d > 1.6 \mu\text{m}$) number concentrations display a decrease with height
9 also in the PBL, due to sedimentation processes (Ferrero et al., 2010).

10

11 **3 Experimental setup**

12 Ground-based and vertical profiles measurements used in this study were conducted at Torre
13 Sarca site which is located on the northern side of Milan ($45^{\circ}31'19''\text{N}$, $9^{\circ}12'46''\text{E}$; within the
14 Milano-Bicocca University campus), in the midst of an extensive conurbation that is the most
15 industrialized and heavily-populated area in the Po Valley. We report here a brief description
16 of the experimental setup and provide relevant references for further details.

17

18 **3.1 Particulate matter bulk composition and number size distribution, and** 19 **gas-phase composition**

20 At ground level, $\text{PM}_{2.5}$ and PM_1 (EN-14907) samples were gravimetrically collected using the
21 FAI-Hydra dual channel Low-Volume-Sampler (LVS; $2.3 \text{ m}^3 \text{ h}^{-1}$, 24 hours of sampling time,
22 PTFE filters for PM_1 , ore-fired Quartz fibre filters for $\text{PM}_{2.5}$, $\varnothing=47 \text{ mm}$), while the aerosol
23 number-size distribution was constantly monitored using an Optical Particle Counter (OPC;
24 Grimm 1.107 “Environcheck”, 31 class-sizes ranging from $0.25 \mu\text{m}$ to $32 \mu\text{m}$). Further details
25 are given in Ferrero et al. (2014).

26 The aerosol chemistry was assessed on $\text{PM}_{2.5}$ samples for the ionic fraction, EC and OC,
27 respectively. For the purpose of ions' analysis, $\text{PM}_{2.5}$ samples were extracted in 3 mL of
28 ultrapure water (Milli-Q[®]; $18.2 \text{ M}\Omega\cdot\text{cm}$) for 20 minutes using an ultrasonic bath (SONICA,
29 Soltec, Italy). The obtained solutions were then analysed using a coupled ion chromatography
30 system consisting of: 1) a Dionex ICS-90 (CS12A-5 Analytical column) with an isocratic

1 elution of methanesulfonic acid (20 Mm; 0.5 mL/min) whose signal was suppressed by means
2 of tetrabutylammonium hydroxide (0.1 M; CMMS III 4 mm MicroMembrane Suppressor) for
3 cations (Na^+ , K^+ , Ca^{++} , Mg^{++} , NH_4^+) and, 2) a Dionex ICS-2000 (AS14A-5 analytical
4 columns) with an isocratic solution of $\text{Na}_2\text{CO}_3/\text{NaHCO}_3$ (8.0 mM/1.0 mM; 1 mL/min) whose
5 signal was suppressed by means of sulphuric acid (0.05 M; AMMS III 2 mm MicroMembrane
6 Suppressor) for anions (F^- , Cl^- , NO_3^- , SO_4^{2-}).

7 EC and OC were determined in $\text{PM}_{2.5}$ using the Thermal Optical Transmission method (TOT,
8 Sunset Laboratory inc.; NIOSH 5040 procedure,
9 <http://www.cdc.gov/niosh/nmam/pdfs/5040f3.pdf>). The organic matter (OM) fraction was
10 then estimated from OC using a coefficient to account for the presence of hetero-atoms (H, O,
11 N, etc.). Following the work of Turpin and Lim (2001), the chosen factor was 1.6 for the
12 urban Torre Sarca site.

13 Finally, meteorological and gas-phase (NO_x , O_3) observations at ground-level were taken
14 from the weather and monitoring stations operated in Milan by the local regional
15 environmental protection agency (ARPA Lombardia).

16

17 **3.2 Size-segregated aerosol composition**

18 From July 14 (8:00 local time LT) to 18 (8:00 LT), 2007, size segregated daytime (8:00 to
19 21:00 LT) and night-time (21:00 to 8:00 LT) aerosol samples were collected by means of a
20 five-stage Berner impactor (LPI 80/0.05) with 50% size cut at 0.05, 0.14, 0.42, 1.2, 3.5 and 10
21 μm aerodynamic diameter. Substrates were off-line analyzed for the determination of the
22 carbonaceous - water soluble organic (WSOC) and water insoluble (WINC) carbon - and
23 soluble inorganic components (NH_4^+ , Na^+ , K^+ , Ca^{2+} , Mg^{2+} , Cl^- , NO_3^- , SO_4^{2-}). Mass-to-carbon
24 ratios of 1.8 and 1.2 were used to convert WSOC to the corresponding mass, WSOM (water-
25 soluble organic matter) and WINC to WINCM (water-insoluble carbonaceous matter),
26 respectively. A complete description of the sampling and analytical methods adopted is
27 reported in Carbone et al. (2010) and references therein. In the analysis presented here, we
28 only used the total mass of aerosol components (sum over size bins).

29

1 **3.3 Lidar-ceilometer profiles**

2 Lidar-ceilometers (called Lidar for brevity in the manuscript) operate on the same physical
3 basis of more complex research-type lidars, but are compact systems, generally with a lower
4 laser energy power, capable of operating 24 hours per day, unattended and in all weather
5 conditions. Initially developed for cloud-base determination, the technology of these system is
6 now mature enough to represent a very convenient and widely used tool for the operational
7 monitoring of the atmospheric aerosol and of relevant meteorological parameters (e.g.
8 Haeffelin et al., 2012).

9 A lidar-ceilometer (Vaisala LD-40) operating at 855 nm collected aerosol profiles at the
10 Milan Torre Sarca site in the January 2007-February 2008 period. The system was switched
11 on during selected dates (and mostly when meteorological conditions allowed the
12 contemporary launch of balloon-borne aerosol instruments, Ferrero et al. 2010), collecting a
13 database of more than 200 days of measurements. During the selected dates, the Lidar-
14 ceilometer operated 24 hours per day, collecting aerosol profiles every 15 seconds that were
15 afterwards averaged over 15 minutes to achieve a better signal-to-noise ratio. Due to the
16 instrumental limitations, the lowest altitude the system can observe is about 60 m. After the
17 background noise is subtracted from the collected backscattered signal, the range-corrected
18 signal (RCS, i.e., the signal S times the square of the system-to-target distance R) is derived to
19 extract information on the aerosol vertical distribution. More details on the system and
20 measurements capabilities can be found in Angelini et al. (2009) and Di Giuseppe et al.
21 (2012).

22

23

24 **4 WRF/Chem model**

25 **4.1 Description and Setup**

26 The 3.4.1 version of the Weather Research and Forecasting model with Chemistry
27 (WRF/Chem), with some updates, is used in order to interpret the observed concentrations of
28 aerosol and its composition at surface and along vertical profile of PBL. WRF/Chem is a
29 coupled on-line model where meteorological and chemical processes are fully consistent
30 (Grell et al., 2005).

1 The model is configured with two 1-way nested domains centred on Northern Italy (Po
2 Valley). The mother domain covers Western Europe with 131×95 cells at a horizontal
3 resolution of 30 km, the nested domain covers Northern Italy with 109×91 cells at a
4 resolution of 10 km. The vertical grid is made of 33 eta levels up to 50 hPa, with first five
5 levels centred approximately at 12, 36, 64, 100 and 140 m above the ground and 12 levels
6 below 1 km.

7 The physical and chemical parameterizations used are the same for the two domains, and are
8 listed in Table 1. These include the Rapid Radiative Transfer Model for short and long wave
9 radiation (Iacono et al., 2008), the Mellor-Yamada Nakanishi-Niino boundary layer
10 parameterization (Nakanishi and Niino, 2006), the Noah Land Surface Model (Chen and
11 Dudhia, 2001), the Morrison cloud microphysics scheme (Morrison et al., 2009), and the
12 Grell 3D ensemble cumulus scheme, which is an update version of the Grell-Devenyi scheme
13 (Grell and Devenyi, 2002). Cumulus clouds feedback with radiation is activated.

14 The gas-phase chemistry is simulated with an updated version of the Regional Atmospheric
15 Chemistry Mechanism (RACM) that includes a wide range of chemical and photolytic
16 reactions for organic and inorganic species (Stockwell et al., 1997). Aerosol parameterization
17 adopted is the Modal Aerosol Dynamic for Europe (Ackermann et al., 1998) that uses three
18 overlapping lognormal modes for Aitken, accumulation and coarse particles. Thermodynamic
19 equilibrium for inorganic species is calculated using the MAR-A module (Saxena et al., 1986;
20 Binkowski and Roselle, 2003). The Secondary Organic Aerosol (SOA) production is
21 calculated using the Volatility Basis Set (VBS) scheme implemented in WRF/Chem by
22 Ahmadov et al. (2012), which include the oxidation of anthropogenic and biogenic VOC
23 currently believed to be important for SOA production (alkanes, alkenes, xylenes, aromatics,
24 isoprene, monoterpenes, and sesquiterpenes). To our knowledge, this study is the first
25 application over Europe of this new parameterization for SOA yield by means of WRF/Chem.
26 Photolysis rates are estimated with the Fast-J scheme (Wild et al., 2000). The dry deposition
27 flux is simulated with the scheme by Wesely et al. (1989), and the dry deposition velocity of
28 organic vapours is assumed to be the 25% that of nitric acid (HNO_3). Cloud chemistry in
29 convective updraft is parameterized following Walcek and Taylor (1986). Wet deposition due
30 to convective and large scale precipitation is also included in our simulations. The aerosol
31 optical properties are calculated online with the package by Barnard et al. (2010), using the
32 volume average internal mixing assumption. We included the direct effect of aerosol on

1 radiation, but the indirect aerosol effects on clouds were switched off since this function is still
2 under testing with the SOA VBS scheme (Tuccella et al., 2015).

3 In order to enhance the understanding of the influence of the upper-level processes on the
4 pollutant budget at surface, we use the diagnostic of the tendency terms in the continuity
5 equation for chemical species following Wong et al. (2009). We extended the original
6 module, which included only some gas-phase compounds, to include aerosol species and
7 processes as well. Diagnosed terms are: emission, horizontal and vertical advection,
8 photochemistry (gases and aerosols), vertical mixing plus dry deposition (these cannot be
9 separated in the WRF/Chem implementation), convective transport, aqueous chemistry, and
10 wet deposition.

11 We have simulated the period from the June 25 to the July 18, 2007, discarding the first 10
12 days as spin up. Simulation on the mother domain uses initial and boundary meteorological
13 conditions provided by the National Center for Environmental Prediction (NCEP) 6-hourly
14 analyses, having a horizontal resolution of $1^\circ \times 1^\circ$. For the mother domain, chemical
15 boundary conditions are provided with WRF/Chem default idealized vertical profiles,
16 representative of Northern hemispheric, mid-latitude and clean environmental conditions
17 (McKeen et al., 2002; Grell et al., 2005; Tuccella et al., 2012), while boundary conditions to
18 the nested domain are provided by the mother domain. The simulations are carried out at 24
19 hours time-slots, starting at 12:00 UTC of each day and then run for 30 hours, with the first 6
20 hours considered as model spin-up. Chemical fields are restarted from previous runs.

21 **4.2 Emissions**

22 Total annual 2007 anthropogenic emissions of nitrogen oxides (NO_x), carbon monoxide (CO),
23 sulphur oxides (SO_x), ammonia (NH_3), Non-Methane Volatile Organic Compounds
24 (NMVOC), unspiciated particulate matter ($\text{PM}_{2.5}$ and coarse PM), primary organic carbon
25 (OC), and elemental carbon (EC) are taken from the Netherlands Organization for Applied
26 Scientific Research (TNO) database (Kuenen et al., 2014). Annual TNO anthropogenic
27 emissions consist of gridded data from ten source types (SNAP sectors) with horizontal
28 resolution of $1/16^\circ$ latitude by $1/8^\circ$ longitude (about $7 \times 7 \text{ km}^2$).

29 TNO emissions are adapted to WRF/Chem following the methodology used by Tuccella et al.
30 (2012), with minor changes derived from the second phase of the Air Quality Modelling
31 Evaluation International Initiative (AQMEII) (Alapaty et al., 2012, Im et al., 2014a,b).

1 Biogenic emissions are calculated online using the Model of Emissions of Gases and Aerosols
2 from Nature (MEGAN) (Guenther et al., 2006). Sea salt flux is calculated online, while dust
3 source is not included.

4

5

6 **5 Results**

7 **5.1 Preliminary analysis of the observations**

8 In Figure 1 time-series of ground-based meteorological and physical-chemical observations
9 performed in Milan in July 5-20, 2007 period are shown. The large scale circulation is
10 illustrated in Figure S1, while the evolution of cloud cover over Northern Italy is illustrated
11 by MODIS-Aqua true colour images in Figure S2. The period starts with a low-pressure
12 system over Germany, rapidly moving Eastward, and allowing a pressure increase over
13 Northern Italy from July 5 to 8, associated with fair weather and sparse clouds. From July 9 to
14 11, a North Atlantic low-pressure system induces a significant increase of cloud cover over
15 Milan with light rain on July 10. From July 12, a wide anticyclonic system forms over the
16 Western Mediterranean, warranting clear sky and stable conditions until July 20 and later.
17 Maximum daily temperature is around 30°C before the Atlantic perturbation, then it increases
18 steadily (from 25° to 35° C) at a rate of ~ 2 °/day from 11 to 15 as the high-pressure system
19 settles. Humidity is high at night (above 70%) on the days following the low-pressure
20 passage, then the atmosphere gradually dries out under the anticyclone.

21 During the period preceding the Atlantic perturbation (July 5-8, 2007), wind is prevalently
22 westerly daytime, forced by the large scale circulation, with wind speed around 2.5-3 m/s.
23 Wind is slowed down to less than 1 m/s at night, because the downward transport of
24 momentum toward the surface is inhibited by the nighttime vertical stratification (Stull, 1988;
25 Whiteman, 1990). Wind speed increases up to 5 m/s at the passage of the low-pressure system
26 (July 9-11, 2007), and it stays above 2 m/s also nighttime. From July 11, when the high-
27 pressure over the Mediterranean begins to settle, the wind field adjusts to a typical mountain-
28 valley breeze regime (Whiteman, 1990). Starting from midnight, the slow (~ 1 m/s) northerly
29 flow gradually accelerates and rotates clockwise, reaching peak speeds of ~ 3 m/s in the
30 afternoon at south-westerly direction, then gradually slows down and return northerly. This
31 wind pattern favours conditions of stagnation and recirculation of air within the valley,

1 allowing the build-up of pollutants from a day to the next. Figure S3 shows the simple
2 stagnation and recirculation indices proposed by Allwine and Whiteman (1994) and confirms
3 that the only ventilated period is that of the Atlantic perturbation.

4 The passage of the Atlantic low-pressure system on July 9-10 marks a sort of “restart” for the
5 atmospheric composition at ground level. Indeed, relatively longer lived (few days) chemical
6 species, such as ozone and PM, first accumulate during the days preceding the perturbation,
7 then are suppressed in perturbed weather, and finally re-accumulate afterwards (Figure 1 c,d).
8 Outside the perturbed period, ozone and nitrogen oxides (NO_x) follow a daily cycle typical of
9 that observed in many urban areas (Mavroidis and Iliá, 2012, and references therein). The
10 primary pollutant nitric oxide (NO) displays a sharp peak during morning rush hours
11 (between 6 and 9 Local Solar Time), then gradually decreases during the day. It displays a
12 secondary small peak during evening rush hours (20-22 LST), then remains at low values
13 until the following morning. Nitrogen dioxide (NO_2) is mainly originated from the oxidation
14 of NO by ozone and peroxy radicals (Jenkin and Clemitshaw, 2000), and displays peaks
15 delayed by ~ 1 hour with respect to those of NO. It shows a plateau between the morning and
16 the evening peak, because concentrations are sustained daytime by photochemistry. The
17 photolysis of NO_2 is the main tropospheric source of atomic oxygen (O) that readily reacts
18 with molecular oxygen (O_2) to produce ozone. Indeed, during daylight hours, NO, NO_2 and
19 O_3 equilibrate on the so called “photostationary equilibrium” on time scales of minutes (Clapp
20 and Jenkin, 2001).

21 Ozone is depleted during the morning rush hours by reaction with NO, then it is
22 photochemically formed during the day and peaks during late afternoon (14-16 LST), and
23 thereafter gradually decreases to lower nighttime levels. In fair weather, the daily cycle of
24 ozone and NO_x is regulated by the solar radiation, the dilution of fresh emissions from the
25 surface in the growing daytime PBL, the vertical mixing with air entrained from the residual
26 layer and the free troposphere above the PBL, and the dry deposition at the surface. Past
27 studies pointed out that the entrainment from ozone-rich residual layer may be as important as
28 the photochemical production in the PBL during pollution events even in urban atmospheres
29 (e.g. Zhang and Rao, 1999). In the present case, the build-up of ozone in the days following
30 the perturbation is evident, but it is difficult to discern the relative role played by the local
31 photochemical production and by the vertical mixing on the ozone trend observed at the
32 surface.

1 Accumulation and cleansing of the atmosphere near the surface is even more evident from
2 aerosol time-series (Figure 1 d-g). $PM_{2.5}$ and PM_1 follow a similar trend, while PM_{10} often
3 show a different behaviour, pointing out the presence of additional sources to the coarse
4 fraction, most probably the erosion and resuspension of soil material by vehicles and wind.
5 The aerosol mass is shown to build up before the Atlantic perturbation (PM_{10} around 20-30
6 $\mu\text{g}/\text{m}^3$) and to abruptly decrease (PM_{10} below 10 $\mu\text{g}/\text{m}^3$) during the low-pressure system
7 passage (probably because of a combination of enhanced ventilation, wet deposition
8 processes, and soil erosion inhibited by increased soil moisture). Afterwards, PM
9 concentration keep increasing after the low-pressure passage (maximum PM_{10} values of more
10 than 60 $\mu\text{g}/\text{m}^3$ reached on July 18-19). Daily cycle of the fine aerosol mass ($PM_{2.5}$ and PM_1)
11 displays similarities with that of NO , in particular a similar morning peak, indicating the
12 important role played by primary emissions. This is confirmed by the analysis of aerosol
13 speciation (Figure 1 e), which shows high values of elemental carbon (EC, 2-4 $\mu\text{g}/\text{m}^3$) and
14 insoluble carbonaceous matter (WINCM, 2-10 $\mu\text{g}/\text{m}^3$). The latter makes, on average, 40-50%
15 of the PM_1 mass (Carbone et al., 2010). Major secondary species are inorganic ions (sulfate,
16 nitrate, and ammonium) and part of the organic matter, which may be associate with its water
17 soluble fraction (WSOM, Carbone et al., 2010). Similarly to ozone, secondary aerosol
18 accumulates during the days preceding and following the perturbation.

19 Cleansing of the atmosphere after the perturbation and subsequent recover of the aerosol load
20 is also clearly visible in the number concentration timeseries. At the passage of the
21 perturbation, aerosol number rapidly decreases by more than an order of magnitude at all
22 observed size ranges, then returns to the pre-perturbation levels on a time scale of about two
23 days. We note, however, differences in the aerosol regime before and after the perturbation.
24 Before the cleansing, the aerosol size distribution is locked to a fixed shape, with no or little
25 daily variability. Conversely, in the stable conditions of July 12-19, it displays a clear daily
26 cycle with a growth towards larger sizes in daytime, and a return to narrower distributions
27 nighttime.

28 As mentioned in sec. 3.3, Lidar observations are only available in the days following the
29 perturbation and give useful indications on the aerosol vertically-resolved infra- and inter-
30 diurnal variability (e.g. Angelini et al., 2009). During the morning hours, a layer of aerosol is
31 formed under the growing boundary layer. There, fresh emissions from the surface are diluted
32 and mixed vertically in the PBL. Throughout the period, but especially on some days such as

1 in the mornings of July 13 and 15, an enhanced layer of aerosol is visible in the upper levels
2 near the top of the PBL. Aerosol is subsequently partly removed in the second half of the day
3 by the mountain breeze, while a residual layer with relatively high aerosol content may
4 survive above the nocturnal PBL (e.g. on July 13, 15, and 16). This layer may potentially be
5 entrained the following morning into the PBL and contribute to the surface aerosol budget.
6 On the last days displayed in Figure 1, a further aerosol layer between 2 and 3 km appears in
7 the Lidar signal. As indicated by increased coarse fraction AOD at Modena AERONET
8 station (Figure S4) and model backtrajectories (Figure S5), it is a Saharan dust incursion
9 which is probably entrained at ground level, as indicated by the enhancement of PM₁₀ levels
10 on days of July 18-19. Since Saharan dust intrusions are not modelled here, these days are
11 excluded from the analysis.

12 From the measurements reported here some questions emerged:

- 13 1. What is the composition of the aerosol layer formed during the day in the upper PBL?
- 14 2. How much of the aerosol burden measured at the ground is due to localized processes and
15 how much is conversely due to processes occurring in the upper PBL and to the
16 subsequent mixing in the lowermost levels? In other words, how important is the interplay
17 between surface and upper layers in shaping the aerosol mass we measure near the
18 ground?
- 19 3. How much may the residual layer above the PBL contribute to the aerosol budget at
20 ground level the next day?

21 We attempted to provide answers to these questions using simulations with the WRF/Chem
22 model and relevant comparison with the observational dataset.

23 **5.2 Model verification against available observations**

24 Before drawing conclusions on the scientific questions outlined at the end of the previous
25 section, we verified our model simulations against the dataset of observations depicted in
26 Figure 1 and only displayed results for the nested domain over Northern Italy, using statistical
27 indices defined in Appendix A as a guidance to quantify model biases.

28 In Figure 2 we compared observed and simulated meteorological variables at ground level in
29 Milan for the period July 5-17, 2007. The temperature is underestimated by about 2.5°C,
30 which is probably due to poorly resolved dynamics and heat fluxes in the urban boundary

1 layer. The overestimation of relative humidity of about 10% is mostly attributable to the
2 underestimation of temperature. Wind speed at 10 m is overestimated by 0.8 m/s and has a
3 relatively low correlation of 0.29 with observations, thus fitting to typical characteristics of
4 current mesoscale models (e.g Misenis and Zhang, 2010). The simulated wind speed is also
5 more variable than that observed as denoted by the Root Mean Square Error (RMSE) of 1.7
6 m/s. The wind direction is generally captured well, in particular the mountain-valley cycles
7 after the passage of the perturbation of July 9.

8 In Figure 3 we show comparison of gas-phase observations and simulation near the ground.
9 The daily cycle of NO is reproduced well ($r = 0.52$), the timings of the morning peak and the
10 subsequent decrease are captured by the model. The magnitude of the morning peak does not
11 show a tendency to underestimate nor to overestimate, while NO values for the rest of the day
12 are underestimated, resulting in a bias of -4.1 ppb (-60%). The model is also able to capture
13 the basic features of the NO₂ daily cycle, i.e. the morning and evening peaks and the
14 minimum at night. However, values are generally underestimated (bias of -8.3 ppb or -34%)
15 and the trend on weekly time scale display much less variability than that observed. Ozone
16 display a very low systematic bias (-2.3 ppb), but less variability than observations (RMSE of
17 11.3 ppb), and a correlation of 0.65. The timing of the daily cycle is captured well, with a
18 maximum in the afternoon, a secondary peak around midnight, and a minimum during the
19 morning rush hour.

20 In Figure 4 we compare PM₁₀ and PM_{2.5} simulated mass to hourly observations at ground.
21 The PM₁₀ trend is qualitatively captured by the model, displaying the sharp decrease at the
22 passage of the perturbation on July 10 and the subsequent gradual accumulation in the
23 following days. This lends confidence in the simulated removal and production terms, and the
24 resulting negative bias is low ($-4 \mu\text{g}/\text{m}^3$ or -10%). The model also captures some of the
25 characteristics of the daily cycle ($r = 0.57$), however the observed signal is quite irregular, and
26 the model does not reproduce all the variability. The negative bias of PM₁₀ could be partly
27 explained by the missing source from soil dust erosion and resuspension caused by traffic in
28 the model. For PM_{2.5} the general features of the comparison are similar to PM₁₀, but the
29 model has a positive bias ($+4 \mu\text{g}/\text{m}^3$ or +70%), mostly attributable to few spurious peaks in
30 the simulation. The overestimation of PM_{2.5} partly compensates and masks the
31 underestimation of coarse particles (PM_{2.5-10}). The comparison of the simulated number size

1 distribution against that observed with the OPC (not shown) suggests that the high bias of
2 $PM_{2.5}$ is attributable to aerosol in the size range 0.5-1 μm .

3 In Figure 5 we show the comparison of simulated $PM_{2.5}$ composition with daily and bi-daily
4 samplings near the ground. In the period precedent to the perturbation (July 5-9), the model
5 underestimates the magnitude of the observed peak of sulfate and ammonium, but it
6 reproduces subsequent “restart” and recovery well. Observed nitrate displays little variability,
7 with a slight decrease at the passage of the perturbation and almost constant levels during the
8 rest of the period. Modelled nitrate has a much more variable behaviour, which seems to be
9 characterized by sudden and irregular pulses. The bi-daily observations indeed suggest that
10 the daily average observation masks much of the underlying variability associated to nitrate.
11 Recently reported hourly measurements of PM composition in the Po Valley indeed confirm
12 the same “pulsed” behaviour of nitrate near the ground, with values near zero during daytime,
13 and irregular peaks at nighttime (Decesari et al., 2014). This highlights the inherent
14 difficulties in simulating the nitrate concentrations at sub-daily frequency. Elemental carbon,
15 being primary and almost hydrophobic, is largely unaffected by the perturbation. This feature
16 is captured by the model, but EC values are underestimated by a factor of two, probably due
17 to underestimated emissions. Interestingly, the bi-daily observations of WINCM (EC plus
18 primary insoluble organic material) display a large diurnal cycle (maximum at night and
19 minimum during the day) which is not captured by the model. Organic carbon trend and
20 magnitude is reproduced quite well, with the exception of a large spurious peak on July 8-9
21 not seen in the observations. The peak is associated with secondary organic aerosol (not
22 shown). The bi-daily observations of soluble organic material (WSOM) do not show the
23 strong daily cycle of primary carbonaceous matter, and confirm a tendency of the model at
24 overestimating the SOA fraction.

25 In Figure 6 we qualitatively compare the Lidar profiles with the simulated $PM_{2.5}$ profiles. A
26 quantitative comparison would require the calculation of optical properties of simulated $PM_{2.5}$
27 and subsequent solution of the Lidar equation (Hodzic et al., 2004). However, a first
28 approximation Lidar signal may be associated to $PM_{2.5}$ mass. The model captures some of the
29 basic features of the previously described aerosol profile cycle observed in this period (sec.
30 5.1). Every morning a plume of fresh aerosol detaches from the ground and follows/traces the
31 growing boundary layer until its maximum extension in the central part of the day. Then, in
32 the afternoon, the mountain-valley breeze cleans the lower PBL (note the abrupt abatement of

1 both the Lidar and the model aerosol signals in the second part of the day), often leaving an
2 upper air aerosol residual layer above. Model simulations also reproduce such residual layers
3 (note the afternoon increase of $PM_{2.5}$ values in the upper levels, particularly visible on July
4 15-16). When such residual layers persist overnight, the Lidar shows these to entrain into the
5 developing PBL the day after (note the merging of the upper level aerosol layers with the
6 growing, aerosol-traced PBL in Figure 6a, particularly evident in the morning of July 14 and
7 15). There are also hints of the same features in model simulations.

8

9 **5.3 Insights into the budget of aerosol vertical profile over Milan**

10 The “chemical restart” caused by the passage of the perturbation on July 9-10, and the
11 following settling of an almost periodic circulation pattern, naturally creates favourable
12 conditions for a study of the processes yielding aerosol production and accumulation in the
13 area of Milan. Our analysis shall now focus on the days following the perturbation (July 12-
14 17).

15 Using model output, we firstly examined the composition of the aerosol layers noted in the
16 Lidar profiles of Figure 6. In Figure 7, we show the composition of $PM_{2.5}$ simulated over
17 Milan. The model predicts a major role played by the primary fraction (unspeciated
18 anthropogenic, black carbon, and primary organic carbon), which is largely responsible for
19 the two rush hours peaks (morning and evening) and the bulk of aerosol mass in the PBL.
20 Fresh emissions are mostly concentrated near the ground and turbulent transport dilutes them
21 in the PBL during the day. A relatively small fraction ($\sim 30\%$) of primary aerosol remains
22 above the PBL overnight and contributes to the upper aerosol layers seen by the Lidar.

23 The sum of secondary species contributes 40-60% of the aerosol mass in the PBL, but with
24 remarkable differences in the vertical distribution of single components. Sulfate and
25 Secondary Organic Aerosol (SOA) start to form and dilute under the PBL a few hours after
26 sunrise, contributing in a relatively homogeneous way to the aerosol column in the PBL.
27 Anthropogenic SOA (ASOA) contributes more than biogenic SOA (BSOA) to the SOA
28 budget. The concentration of those secondary species are similar also above the PBL, thus
29 significantly contributing to the upper aerosol layers. ASOA are slightly more persistent than
30 BSOA and sulfate in the free troposphere.

1 Nitrate displays a profile substantially different compared to other species, with enhanced
2 concentrations in the upper part of the PBL formed during the central part of the day. These
3 concentrations may largely exceed those found near the ground (i.e. on July 13, 16, 17).
4 Moreover, nitrate is predicted to be the major secondary species contributing to the formation
5 of the residual aerosol layers above the PBL. Enhanced upper level concentrations of nitrate
6 into PM_{10} were also reported at Monte Cimone (a mountain peak of 2160 m at the southern
7 border of the Po Valley) by Carbone et al. (2010, 2014).

8 In Figure 8 we show the maps of simulated sulfate and nitrate over the Po Valley on July 13,
9 2007 at 16 LST at the surface and at 750 m height. It can be seen that the main features of the
10 composition of the aerosol profile outlined above are not peculiar of the Milan area, but are
11 suggested to be representative of the larger area of the Po Valley.

12 In order to better understand the processes underlying the predicted characteristics of the
13 aerosol over Milan, we analysed the terms of the continuity equation for chemical species.
14 Budget terms considered are emission, horizontal and vertical advection, chemistry, turbulent
15 mixing and dry deposition. Terms related to cloud processes (convection, aqueous chemistry,
16 wet deposition) make a very small contribution in the dry period under investigation and are
17 not shown to improve the figure's clarity. In Figure 9 we show the vertical profile of the
18 budget terms for sulfate and nitrate at 16 local time of July 13 over Milan. For sulfate, the
19 dominant terms are those related to advection, indicating the presence of spatially distributed
20 sources and a relatively long lifetime, making it a regional scale pollutant. Locally, sulfate is
21 both directly emitted and produced by secondary pathways throughout the PBL. Turbulent
22 mixing distributes it vertically in the PBL and dry deposition removes it from the atmosphere
23 near the ground, determining an almost homogeneous sulfate profile in the PBL. Conversely,
24 nitrate has relatively low contribution from advection, while the largest terms are chemistry
25 and vertical mixing. In the simulation, nitrate is produced only in the upper half of the PBL
26 and destroyed in the lower half. The vertical transition between the nitrate destruction and
27 production zone is quite sharp. Turbulent mixing is nearly in equilibrium with chemical
28 production, indicating that model simulates a very rapid adjustment to the thermodynamic
29 equilibrium for the sulfate-nitrate-ammonium system. This results in nitrate concentrations
30 higher in the upper part of the PBL compared to the lower part.

31 Similar to nitrate, SOA also displays an enhanced net chemical production in the upper part of
32 the PBL and destruction in the lower part (Figure 10), but since the chemical and vertical

1 mixing terms are of the same order of the advection terms the resulting vertical profile is
2 almost constant with height, similar to that of sulfate.

3 Further insights into the simulated sharp transition to an environment favourable to nitrate
4 formation in the upper part of the PBL, is investigated by means of several model sensitivity
5 tests as outlined in Table 2. In Figure 10 we first look at the gas phase precursor of nitrate,
6 nitric acid (HNO_3). The left panel shows the vertical profile of the budget terms for HNO_3 at
7 the same instant of Figure 9. The chemical and vertical mixing terms mirror those of
8 particulate nitrate, resulting in a decreasing concentration profile with height. The right panel
9 of Figure 9 shows the budget profile from a sensitivity simulation where aerosol chemistry is
10 switched off (AERO, see Table 2). The chemistry and vertical mixing terms are greatly
11 reduced and are the same order of magnitude of advective terms, indicating that the sharp
12 gradients in net chemical production of HNO_3 (and nitrate) are dominated by aerosol
13 processes, and not by gas-phase processes.

14 In Figure 12 we provide further elements to evaluate the simulated particulate nitrate
15 thermodynamics. Ambient relative humidity increases with height in the PBL, from a
16 minimum of ~50% near the ground to a maximum of ~80% at an altitude of 1000 m (~400 m
17 below the PBL top). The nitrate chemical production term shown in Figure 9 is reported for
18 ease of comparison, and displays the already noted peak between 500 and 1000 m. The sulfate
19 ratio (ratio of total ammonia and sulfate) is well above the threshold of 2 along the profiles
20 (not shown), thus suitable for particulate nitrate formation (Seinfeld and Pandis, 2006). The
21 profile of equilibrium constants for both the aqueous and solid nitrate increase with height, in
22 response to a decreasing temperature profile (not shown), indicating that conversion of nitric
23 acid to particulate is favoured with increasing height. However, no sharp transitions,
24 correlated to the nitrate net chemical term, can be noticed in the profiles of those equilibrium
25 constants.

26 The profile of ammonium nitrate's deliquescence relative humidity (DRH) helps disclosing
27 the possible reason for such a transition. At ground level, ambient RH is well below the
28 ammonium nitrate DRH, indicating an environment thermodynamically favourable only to
29 the solid form of nitrate. However, since the RH gradient with height is steeper than that of
30 DRH, the two curves intersect at an altitude of ~500 m, and then again at ~1300 m, because of
31 the RH decrease near the PBL top. Ambient RH is thus higher than ammonium nitrate DRH
32 in the same altitude range (~500-1000 m) where the nitrate net chemical production peaks.

1 This indicates that, over Milan and in the period under consideration, the nitrate chemical
2 production is dominated by aqueous conversion of nitric acid to nitrate ion, condition that is
3 reached only in the upper part of the PBL, where RH levels are high enough to sustain the
4 formation of an aqueous solution containing nitrate. Although the real multicomponent DRH
5 point will differ from that of pure nitrate, it is known that the DRH of mixtures is always
6 lower than that of pure salts (Seinfeld and Pandis, 2006). The thickness of the layer
7 favourable to aqueous nitrate formation deducible from Figure 12 may thus be regarded as a
8 conservative lower estimate. During daytime, the nitrate formed in the upper boundary layer
9 re-evaporates back to the gas phase when brought to the ground by vertical motions, and
10 that's the origin of the inhomogeneous vertical profile of nitrate. For further discussion on
11 how much the upper aerosol layer contributes to ground PM we point the reader to the next
12 paragraph.

13 The budget analysis we have presented so far reveals a complex interplay between chemical
14 processes and vertical mixing taking place at different altitude ranges. In order to better
15 quantify the impact of chemical production at upper layers on particulate matter at ground
16 level, we perform three tests alternatively switching on/off the chemical process at selected
17 altitude ranges (namely within the lower half of the PBL, the upper half of the PBL and above
18 the PBL, see Table 2). Results are shown in Figure 13 for $PM_{2.5}$, and its components sulfate,
19 nitrate and SOA. In the figure, the contribution to the ground $PM_{2.5}$ of the chemical processes
20 in the different altitude ranges is positive/negative when the associated sensitivity line is
21 below/above the CTRL. For $PM_{2.5}$, we have found that chemical process in all regions
22 positively contribute to the ground level concentration. During the first days after the passage
23 of the perturbation, the shutdown of secondary chemical formation makes very little
24 difference, indicating a dominance of primary emissions. As time goes by, secondary
25 processes gain importance, but primary fraction remains the main driver of $PM_{2.5}$
26 concentration even after a week. Interestingly, the magnitude of the relative contribution of
27 the different layers (lower PBL, upper PBL, above PBL) to ground level $PM_{2.5}$ is comparable,
28 and of the order of up to 7-8 $\mu\text{g}/\text{m}^3$ each, on hourly basis. Exceptions are noted on afternoons
29 of July 13 and 16, when a negative contribution from secondary processes in the lower PBL is
30 simulated (note the blue dashed line above the red line). These peaks are associated with the
31 nitrate sink in the lower PBL (see panel c). Sulfate has an identical contribution from lower
32 and upper PBL chemical production, and may also have a very important contribution from
33 the region above the PBL, even higher than processes in the PBL (e.g. on July 17). SOA

1 budget is similar to that of sulfate, but with an enhanced contribution from PBL processes
2 versus those above it. As expected, nitrate displays distinctive features. Chemical production
3 in the lower PBL positively contributes to ground level concentration in the first part of the
4 day, then in the afternoon results in a net destruction. On the other hand, processes in the
5 upper PBL and above PBL always positively contribute to the ground level nitrate
6 concentrations.

7 A further quantitative assessment of the impact of upper aerosol layers on ground
8 concentrations can be estimated combining information in Figure 14 and Figure 6. In Figure
9 14 we show the time-series of the difference in the simulated $PM_{2.5}$ profile between APBL
10 and CTRL runs. When a residual layer is visible, we may roughly estimate from the figure the
11 related change near the surface on the subsequent morning. We focus our attention on July 17,
12 when the presence of a residual layer is clearly visible. The concentration change (APBL –
13 CTRL) in the residual layer is about 8-10 $\mu\text{g}/\text{m}^3$. The following morning the concentration
14 change near the surface is 4-5 $\mu\text{g}/\text{m}^3$, thus we may estimate a 50% sensitivity of ground $PM_{2.5}$
15 to a change in the residual layer. In Figure 6b, we see that on July 17 the $PM_{2.5}$ concentration
16 in residual layer is 20-24 $\mu\text{g}/\text{m}^3$, thus the expected impact on hourly concentrations near the
17 ground is of the order of 10-12 $\mu\text{g}/\text{m}^3$, or about 40% of the $PM_{2.5}$ concentration near the
18 ground. This is the extreme case in the short period analyzed here, but gives a feeling of the
19 potential importance that entrainment of aerosol layers aloft may occasionally have on $PM_{2.5}$
20 observed near the surface.

21

22 **6 Conclusions**

23 The object of this study is the analysis of the role played by the combination of chemical and
24 dynamical processes occurring throughout and above the PBL in determining the aerosol
25 concentration and composition we observe near the ground. We analyzed the observations of
26 the atmospheric composition during a period of two weeks carried out in Milan (Northern
27 Italy) in July 2007. The period was characterized by the passage of a perturbation that
28 favoured cleansing of the Po Valley, providing a natural “chemical restart”. After the
29 perturbation, stable high-pressure conditions determined the establishment of a nearly
30 repetitive meteorological pattern, driven by a mountain-valley breeze system, that allowed for
31 a gradual re-accumulation of pollutants.

1 Lidar observations after the “chemical restart” revealed intriguing features of the aerosol
2 vertical profile over Milan. Every morning, a plume of fresh emissions from the ground is
3 dispersed in the growing convective boundary layer. In the afternoon, an enhanced aerosol
4 layer appears in the upper part of the PBL, while in the evening the bottom part of the PBL is
5 cleansed by the mountain breeze. A residual aerosol layer may form and survive the night
6 above the PBL, and may be entrained again down to the ground the day after. We investigated
7 how this “vertical” sequence of processes affect the aerosol concentrations observed at ground
8 level.

9 With the help of simulations from the state-of-art online meteorology-chemistry model
10 WRF/Chem we attempted to answer three main questions suggested by the observations. The
11 questions and the relative answers are summarized here below:

- 12 • What is the composition of the aerosol layer formed during the day in the upper PBL?
13 Model simulations suggest that 40-60% of the fine aerosol in Milan’s summer PBL is
14 of primary origin, consistently with previous studies (e.g. Carbone et al., 2010). This
15 primary fraction displays a decreasing concentration profile with height in the PBL,
16 since the sources are concentrated near the ground and species are vertically mixed by
17 turbulence. Sulfate and secondary organic aerosol are produced throughout the PBL
18 and have a nearly homogeneous profile there. Nitrate and ammonium have a distinct
19 profile, with enhanced values in the upper PBL, where concentrations may be much
20 higher than those near the ground. The low temperature and the relative humidity
21 above the ammonium nitrate deliquescence point in the upper PBL is thought to
22 determine this peculiar profile. Nitrate is the major component of the upper PBL
23 aerosol layer, contributing up to 30% of the aerosol mass.
- 24 • How much of the aerosol burden measured at the ground is due to localized processes
25 and how much is conversely due to processes occurring in the upper PBL and to the
26 subsequent mixing in the lowermost levels? In other words, how important is the
27 interplay between surface and upper layers in shaping the aerosol mass we measure
28 near the ground?
29 For PM_{2.5} mass, our calculations indicate that in the upper PBL secondary aerosol are
30 formed and then mixed in the PBL by turbulence. The importance of the secondary
31 fraction increases with the aging of air masses, as shown by the progression of days

1 from the “chemical restart”. A week after the perturbation, secondary PM_{2.5} produced
2 in the upper PBL may contribute up to 7-8 µg/m³ (or 25%) to ground level hourly
3 concentrations. Sulfate and SOA production is equally shared by bottom and upper
4 PBL, while nitrate is mostly produced in the upper PBL, the bottom PBL acting as a
5 sink during the afternoon.

- 6 • How much may the residual layer above the PBL contribute to the aerosol budget at
7 ground level the next day?

8 It is calculated that the chemical production above the PBL significantly impacts
9 aerosol levels near the ground, sometimes overtaking the contribution from the
10 production term in the PBL (especially for sulfate and SOA). We estimate that the
11 residual layer above the PBL, which is formed by both primary and secondary species,
12 may occasionally contribute up to 10-12 µg/m³ (or 40%) to ground level PM_{2.5} hourly
13 concentrations during the following morning.

14 The peculiar features of the vertical profile of aerosol nitrate have already emerged in past
15 studies. Neuman et al. (2003) reported aircraft observations of increasing nitrate profiles with
16 height, attributing them to the favourable lower temperature in the upper layers, compared to
17 bottom PBL, due to the conversion of nitric acid to aerosol nitrate. We confirm their
18 conclusion, and add that a key role in shaping the aerosol nitrate production profile is played
19 by the relative humidity. In particular, nitrate production may be enhanced when RH is above
20 the ammonium nitrate deliquescence point.

21 This study has put emphasis on some less obvious and recognized aspects of the aerosol
22 vertical profile budget. Since it is based on the analysis of a short period of high pressure
23 conditions in summer over the area of Milan, further analyses are recommended for winter
24 periods and different meteorological and geographical conditions. Moreover, it clearly
25 underlines the fact that the interplay between chemical and dynamical processes must be
26 considered when interpreting atmospheric chemistry observations near the ground, and that
27 more observational constraints (e.g. profiles of the aerosol composition in and above the PBL)
28 would certainly be helpful to achieve a better simulation of those processes.

29
30

1 **Appendix A: definition of statistical indices used in model to observations** 2 **comparison**

3 Let Obs_i and Mod_i be the observed and modeled values at time i , and N the number of
4 observations.

- 5 • The Pearson's Correlation (r):

$$6 \quad r = \frac{1}{N} \sum_{i=1}^N Z_i (Mod) \cdot Z_i (Obs)$$
$$7 \quad Z(X) = \frac{X - \langle X \rangle}{\sigma_X}$$

8 where X is a generic vector, $Z(X)$ is its standard score, and σ_X is the standard
9 deviation.

- 10 • Bias:

$$11 \quad Bias = \frac{1}{N} \sum_{i=1}^N Mod_i - Obs_i$$

- 12 • Normalized Mean Bias (NMB):

$$13 \quad NMB = \frac{1}{N} \sum_{i=1}^N \frac{Mod_i - Obs_i}{Obs_i} \times 100$$

- 14 • Root Mean Square Error (RMSE):

$$15 \quad RMSE = \sqrt{\frac{1}{N} \sum_{i=1}^N (Mod_i - Obs_i)^2}$$

16 **Acknowledgements**

17 This work was partly funded by the Italian Space Agency (ASI) within the QUITSAT
18 (contract I/035/06/0) project. G. Curci and P. Tuccella are supported by ASI in the frame of
19 PRIMES project (contract I/017/11/0). The authors are extremely thankful to the Euro
20 Mediterranean Centre on Climate Change (CMCC) for having made available the
21 computational resources needed to complete this work. Meteorological and gas-phase

1 observations near the ground are taken from the weather station operated in Milan by the
2 regional environmental agency (ARPA Lombardia). The authors gratefully acknowledge the
3 Wetterzentrale, the NOAA Air Resources Laboratory (ARL), the AERONET network, the
4 MODIS Rapid Response system, the Barcelona Supercomputing Center for the material used
5 in the online supplement to this manuscript.

6

1 **References**

- 2 Aan de Brugh, J. M. J., Schaap, M., Vignati, E., Dentener, F., Kahnert, M., Sofiev, M.,
3 Huijnen, V., and Krol, M. C.: The European aerosol budget in 2006, *Atmos. Chem. Phys.*, 11,
4 1117-1139, doi:10.5194/acp-11-1117-2011, 2011.
- 5 Aan de Brugh, J. M. J., Henzing, J. S., Schaap, M., Morgan, W. T., van Heerwaarden, C. C.,
6 Weijers, E. P., Coe, H., and Krol, M. C.: Modelling the partitioning of ammonium nitrate in
7 the convective boundary layer, *Atmos. Chem. Phys.*, 12, 3005-3023, doi:10.5194/acp-12-
8 3005-2012, 2012.
- 9 Ackermann, I. J., Hass, H., Memmsheimer, M., Ebel, A., Binkowski, F. S., and Shankar, U.:
10 Modal aerosol dynamics model for Europe: development and first applications, *Atmos.*
11 *Environ.*, 32(17), 2981–2999, doi:10.1016/S1352-2310(98)00006-5, 1998.
- 12 Ahmadov, R., McKeen, S. A., Robinson, A. L., Bahreini, R., Middlebrook, A. M., de Gouw,
13 J. A., Meagher, J., Hsie, E.-Y., Edgerton, E., Shaw, S., and Trainer, M.: A volatile basis set
14 model for summertime secondary organic aerosols over the eastern United States in 2006, *J.*
15 *Geophys. Res.*, 117, D06301, doi:10.1029/2011JD016831, 2012.
- 16 Alapaty, K. V., Mathur, R., Pleim, J. E., Hogrefe, C., Rao, S. T., Ramaswamy, V., Galmarini,
17 S., Schapp, M., Vautard, R., Makar, R., Baklanov, A., Kallos, G., Vogel, B., and Sokhi, R.:
18 New Directions: Understanding Interactions of Air Quality and Climate Change at Regional
19 Scales, *Atmos. Environ.*, Elsevier Science Ltd, New York, NY, 49(3):1-424, 2012.
- 20 Allwine, K. J., and Whiteman, C. D.: Single-station integral measures of atmospheric
21 stagnation, recirculation and ventilation. *Atmos. Environ.*, 28, 713-721, 1994.
- 22 Andreani-Aksoyoglu, S., Prévot, A. S. H., Baltensperger, U., Keller, J., and Dommen, J. :
23 Modeling of formation and distribution of secondary aerosols in the Milan area (Italy). *J.*
24 *Geophys. Res.*, 109, D05306, doi:10.1029/2003JD004231, 2004.
- 25 Angelini, F., Barnaba, F., Landi, T. C., Caporaso, L., and Gobbi, G. P.: Study of atmospheric
26 aerosols and mixing layer by LIDAR. *Radiat. Prot. Dosim.*, 137, 275-279, 2009.
- 27 Baltensperger, U., Streit, N., Weingartner, E., Nyeki, S., Prévot, A. S. H., Van Dingenen, R.,
28 Virkkula, A., Putaud, J.-P., Even, A., ten Brink, H., Blatter, A., Neftel, A., and Gaggeler, H.
29 W.: Urban and rural aerosol characterization of summer smog events during the PIPAPO field

1 campaign in Milan, Italy. *J. Geophys. Res.*, 107, D22, 8193, doi:10.1029/2001JD001292,
2 2002.

3 Barnaba, F. and Gobbi, G. P.: Aerosol seasonal variability over the Mediterranean region and
4 relative impact of maritime, continental and Saharan dust particles over the basin from
5 MODIS data in the year 2001, *Atmos. Chem. Phys.*, 4, 2367-2391, doi:10.5194/acp-4-2367-
6 2004, 2004.

7 Barnaba, F., Gobbi, G. P., and de Leeuw, G.: Aerosol stratification, optical properties and
8 radiative forcing in Venice (Italy) during ADRIEX. *Q. J. R. Meteorol. Soc.*, 133, 47-60, 2007.

9 Barnaba, F., Putaud, J.-P., Gruening, G., dell'Acqua, A., and Dos Santos, S.: Annual cycle in
10 co-located in situ, total-column, and height-resolved observations in the Po Valley (Italy):
11 Implications for ground-level particulate matter mass concentration estimation from remote
12 sensing. *J. Geophys. Res.*, 115, D19209, doi:10.1029/2009JD013002, 2010.

13 Barnaba, F., Angelini, F., Curci, G., and Gobbi, G. P.: An important fingerprint of wildfires
14 on the European aerosol load, *Atmos. Chem. Phys.*, 11, 10487-10501, doi:10.5194/acp-11-
15 10487-2011, 2011.

16 Baertsch-Ritter, N., Prevot, A. S. H., Dommen, J., Andreani-Aksoyoglu, S., and Keller, J.:
17 Model study with UAM-V in the Milan area (I) during PIPAPO: simulations with changed
18 emissions compared to ground and airborne measurements. *Atmos. Environ.*, 37, 4133-4147,
19 2003.

20 Baertsch-Ritter, N., Keller, J., Dommen, J., and Prevot, A. S. H.: Effects of various
21 meteorological conditions and spatial emissionresolutions on the ozone concentration and
22 ROG/NOx limitationin the Milan area (I), *Atmos. Chem. Phys.*, 4, 423-438, doi:10.5194/acp-
23 4-423-2004, 2004.

24 Beelen, R., Raaschou-Nielsen, O., Stafoggia, M., Andersen, Z. J., Weinmayr, G., Hoffmann,
25 B., Wolf, K., Samoli, E., Fischer, P., Nieuwenhuijsen, M., Vineis, P., Xun, W. W.,
26 Katsouyanni, K., Dimakopoulou, K., Oudin, A., Forsberg, B., Modig, L., Havulinna, A. S.,
27 Lanki, T., Turunen, A., Oftedal, B., Nystad, W., Nafstad, P., De Faire, U., Pedersen, N. L.,
28 Östenson, C.-G., Fratiglioni, L., Penell, J., Korek, M., Pershagen, G., Eriksen, K. T., Overvad,
29 K., Ellermann, T., Eeftens, M., Peeters, P. H., Meliefste, K., Wang, M., Bueno-de-Mesquita,
30 B., Sugiri, D., Krämer, U., Heinrich, J., de Hoogh, K., Key, T., Peters, A., Hampel, R.,
31 Concin, H., Nagel, G., Ineichen, A., Schaffner, E., Probst-Hensch, N., Künzli, N., Schindler,

1 C., Schikowski, T., Adam, M., Phuleria, H., Vilier, A., Clavel-Chapelon, F., Declercq, C.,
2 Grioni, S., Krogh, V., Tsai, M.-Y., Ricceri, F., Sacerdote, C., Galassi, C., Migliore, E., Ranzi,
3 A., Cesaroni, G., Badaloni, C., Forastiere, F., Tamayo, I., Amiano, P., Dorronsoro, M.,
4 Katsoulis, M., Trichopoulou, A., Brunekreef, B., Hoek, G.: Effects of long-term exposure to
5 air pollution on natural-cause mortality: an analysis of 22 European cohorts within the
6 multicentre ESCAPE project, *The Lancet*, 383, 785-795, doi:10.1016/S0140-6736(13)62158-
7 3, 2014.

8 Binkowski, F. S., and Roselle, S. J.: Models-3 Community Multiscale Air Quality (CMAQ)
9 model aerosol component, 1, Model description, *J. Geophys. Res.*, 108(D6), 4183,
10 doi:10.1029/2001JD001409, 2003.

11 Carbone, C., Decesari, S., Mircea, M., Giulianelli, L., Finessi, E., Rinaldi, M., Fuzzi, S.,
12 Marinoni, A., Duchi, R., Perrino, C., Sargolini, T., Vardè, M., Sprovieri, F., Gobbi, G. P.,
13 Angelini, F., and Facchini, M. C.: Size-resolved aerosol chemical composition over the Italian
14 Peninsula during typical summer and winter conditions, *Atmos. Environ.*, 44, 5269-5278,
15 2010.

16 Carbone, C., Decesari, S., Paglione, M., Giulianelli, L., Rinaldi, M., Marinoni, A.,
17 Cristofanelli, P., Didiodato, A., Bonasini, P., Fuzzi, S., and Facchini, M. C.: 3-year chemical
18 composition of free tropospheric PM₁ at the Mt. Cimone GAW global station e South Europe
19 e 2165 m a.s.l., *Atmos. Environ.*, 87, 218-227, 2014.

20 Carnevale, C., Decanini, E., and Volta, M.: Design and validation of a multiphase 3D model
21 to simulate tropospheric pollution. *Sci. Total Environ.*, 390, 166-176, 2008.

22 Chen, F., and Dudhia, J.: Coupling an advanced land-surface/hydrology model with the Penn
23 State/NCAR MM5 modeling system, Part I: Model description and implementation, *Mon.*
24 *Weather Rev.*, 129, 569–585, doi:10.1175/1520-0493(2001)129<0569:CAALSH>2.0.CO;2,
25 2001.

26 Chu, D. A., Kaufman, Y. J., Zibordi, G., Chern, J. D., Mao, J., Li, C., and Holben, B. N.:
27 Global monitoring of air pollution over land from the Earth Observing System-Terra
28 Moderate Resolution Imaging Spectroradiometer (MODIS). *J. Geophys. Res.*, 108, D21,
29 4661, doi:10.1029/2002JD003179, 2003.

30 Clapp, L. J., and Jenkin, M. E.: Analysis of the relationship between ambient levels of O₃,
31 NO₂ and NO as a function of NO_x in the UK. *Atmos. Environ.*, 35, 6391-6405, 2001.

1 Cook, J., Highwood, E. J., Coe, H., Formenti, P., Haywood, J. M., and Crosier, J.: A
2 comparison of aerosol optical and chemical properties over the Adriatic and Black Seas
3 during summer 2004: Two case-studies from ADRIEX. *Q. J. R. Meteorol. Soc.*, 133, 33-45,
4 2007.

5 Crosier, J., Allan, J. D., Coe, H., Bower, K. N., Formenti, P., and Williams, P. I.: Chemical
6 composition of summertime aerosol in the Po Valley (Italy), northern Adriatic and Black Sea.
7 *Q. J. R. Meteorol. Soc.*, 133, 61-75, 2007.

8 Daher, N., Ruprecht, A., Invernizzi, G., De Marco, C., Miller-Schulze, J., Heo, J. B., Shafer,
9 M. M., Shelton, B. R., Schauer, J. J., and Sioutas, C.: Characterization, sources and redox
10 activity of fine and coarse particulate matter in Milan, Italy. *Atmos. Environ.*, 49, 130-141,
11 2012.

12 Decesari, S., Facchini, M. C., Matta, E., Lettini, F., Mircea, M., Fuzzi, S., Tagliavini, E., and
13 Putaud J.-P.: Chemical features and seasonal variation of fine aerosol water-soluble organic
14 compounds in the Po Valley, Italy. *Atmos. Environ.*, 35, 3691-3699, 2001.

15 Decesari, S., Allan, J., Plass-Duelmer, C., Williams, B. J., Paglione, M., Facchini, M. C.,
16 O'Dowd, C., Harrison, R. M., Gietl, J. K., Coe, H., Giulianelli, L., Gobbi, G. P.,
17 Lanconelli, C., Carbone, C., Worsnop, D., Lambe, A. T., Ahern, A. T., Moretti, F.,
18 Tagliavini, E., Elste, T., Gilge, S., Zhang, Y., and Dall'Osto, M.: Measurements of the aerosol
19 chemical composition and mixing state in the Po Valley using multiple spectroscopic
20 techniques, *Atmos. Chem. Phys.*, 14, 12109-12132, doi:10.5194/acp-14-12109-2014, 2014.

21 de Meij, A., Wagner, S., Cuvelier, C., Dentener, F., Gobron, N., Thunis, P., and Shaap, M. :
22 Model evaluation and scale issues in chemical and optical aerosol properties over the greater
23 Milan area (Italy), for June 2001. *Atmos. Res.*, 85, 243-267, 2007.

24 de Meij, A., Thunis, P., Bessagnet, B., and Cuvelier, C.: The sensitivity of CHIMERE model
25 to emissions reduction scenarios on air quality in Northern Italy. *Atmos. Environ.*, 43, 1897-
26 1907, 2009.

27 Di Carlo, P., Pitari, G., Mancini, E., Gentile, S., Pichelli, E., and Visconti, G.: Evolution of
28 surface ozone in central Italy based on observations and statistical model. *J. Geophys. Res.*,
29 112, D10316, doi:10.1029/2006JD007900, 2007.

1 Di Giuseppe, F., Riccio, A., Caporaso, L., Bonafe, G., Gobbi, G. P., Angelini, F.: Automatic
2 detection of atmospheric boundary layer height using ceilometer backscatter data assisted by a
3 boundary layer model. *Q. J. R. Meteorol. Soc.*, 138, 649–663, doi:10.1002/qj.964, 2012.

4 Dommen, J., Prévot, A. S. H., Neininger, B., and Baumle, M.: Characterization of the
5 photooxidant formation in the metropolitan area of Milan from aircraft measurements. *J.*
6 *Geophys. Res.*, 107, D22, 8197, doi:10.1029/2000JD000283, 2002.

7 Dosio, A., Galmarini, S., and Graziani, G.: Simulation of the circulation and related
8 photochemical ozone dispersion in the Po plains (northern Italy): Comparison with the
9 observation of a measuring campaign. *J. Geophys. Res.*, 107, D18, 8189,
10 doi:10.1029/2000JD000046, 2002.

11 Duong, H. T., Sorooshian, A., Craven, J. S., Hersey, S. P., Metcalf, A. R., Zhang, X., Weber,
12 R. J., Jonsson, H., Flagan, R. C., and Seinfeld, J. H.: Water-soluble organic aerosol in the Los
13 Angeles Basin and outflow regions: Airborne and ground measurements during the 2010
14 CalNex field campaign. *J. Geophys. Res.*, 116, D00V04, doi:10.1029/2011JD016674, 2011.

15 EC: Directive 2008/50/EC of the European Parliament and of the Council of 21 May 2008 on
16 Ambient Air Quality and Cleaner Air for Europe, 2008.

17 Estellés, V., Martínez-Lozano, J. A., Pey, J., Sicard, M., Querol, X., Esteve, A. R., Utrillas,
18 M. P., Sorribas, M., Gangoiti, G., Alastuey, A., and Rocadenbosch, F.: Study of the
19 correlation between columnar aerosol burden, suspended matter at ground and chemical
20 components in a background European environment, *J. Geophys. Res.*, 117, D04201,
21 doi:10.1029/2011JD016356, 2012.

22 Ferrero, L., Perrone, M. G., Petraccone, S., Sangiorgi, G., Ferrini, B. S., Lo Porto, C., Lazzati,
23 Z., Cocchi, D., Bruno, F., Greco, F., Riccio, A., and Bolzacchini, E.: Vertically-resolved
24 particle size distribution within and above the mixing layer over the Milan metropolitan area,
25 *Atmos. Chem. Phys.*, 10, 3915-3932, doi:10.5194/acp-10-3915-2010, 2010.

26 Ferrero, L., Riccio, A., Perrone, M. G., Sangiorgi, G., Ferrini, B. S., and Bolzacchini, E.:
27 Mixing height determination by tethered balloon-based particle soundings and modelling
28 simulations. *Atmos. Res.*, 102, 145-156, 2011.

29 Ferrero, L., Cappelletti, D., Moroni, B., Sangiorgi, G., Perrone, M. G., Crocchianti, S., and
30 Bolzacchini, E.: Wintertime aerosol dynamics and chemical composition across the mixing
31 layer over basin valleys, *Atmos. Environ.*, 56, 143-153, 2012.

1 Ferrero, L., Castelli, M., Ferrini, B. S., Moscatelli, M., Perrone, M. G., Sangiorgi, G., Rovelli,
2 G., D'Angelo, L., Moroni, B., Scardazza, F., Mocnik, G., Bolzacchini, E., Petitta, M., and
3 Cappelletti, D.: Impact of black carbon aerosol over Italian basin valleys: high resolution
4 measurements along vertical profiles, radiative forcing and heating rate, *Atmos. Chem. Phys.*
5 *Discuss.*, 14, 541-591, doi:10.5194/acpd-14-541-2014, 2014.

6 Grell, G. A. and Devenyi, D.: A generalized approach to parameterizing convection
7 combining ensemble and data assimilation techniques, *Geophys. Res. Lett.*, 29, 38-1, 38-4,
8 doi:10.1029/2002GL015311, 2002.

9 Grell, G. A., Peckham, S. E., McKeen, S., Schmitz, R., Frost, G., Skamarock, W. C., and
10 Eder, B.: Fully coupled “online” chemistry within the WRF model, *Atmosph. Env.*, 39, 6957-
11 6975, 2005.

12 Guenther, A., Karl, T., Harley, P., Wiedinmyer, C., Palmer, P. I., and Geron, C.: Estimates of
13 global terrestrial isoprene emissions using MEGAN (Model of Emissions of Gases and
14 Aerosols from Nature), *Atmos. Chem. Phys.*, 6, 3181-3210, doi:10.5194/acp-6-3181-2006,
15 2006.

16 Haeffelin M., Angelini, F., Morille, Y., Martucci, G., Frey, S., Gobbi, G. P., Lolli, S.,
17 O'Dowd, C. D., Sauvage, L., Xueref-Rémy, I., Wastine, B., Feist, D. G.: Evaluation of
18 mixing-height retrievals from automatic profiling lidars and ceilometers in view of future
19 integrated networks in Europe, *Boundary Layer Meteorology* 143, 49-75, 2012.

20 Hamed, A., Joutsensaari, J., Mikkonen, S., Sogacheva, L., Dal Maso, M., Kulmala, M.,
21 Cavalli, F., Fuzzi, S., Facchini, M. C., Decesari, S., Mircea, M., Lehtinen, K. E. J., and
22 Laaksonen, A.: Nucleation and growth of new particles in Po Valley, Italy, *Atmos. Chem.*
23 *Phys.*, 7, 355-376, doi:10.5194/acp-7-355-2007, 2007.

24 Harrison, R. M., and Yin, J.: Particulate matter in the atmosphere: which particle properties
25 are important for its effects on health? *Sci. Total Environ.*, 249, 85-101, 2000.

26 He, T.-Y., Stanič, S., Gao, F., Bergant, K., Veberič, D., Song, X.-Q., and Dolžan, A.:
27 Tracking of urban aerosols using combined LIDAR-based remote sensing and ground-based
28 measurements. *Atmos. Meas. Tech.*, 5, 891-900, doi:10.5194/amt-5-891-2012, 2012.

29 Heald, C. L., Jacob, D. J., Turquety, S., Hudman, R. C., Weber, R. J., Sullivan, A. P., Peltier,
30 R. E., Atlas, E. L., de Gouw, J. A., Warneke, C., Holloway, J. S., Neuman, J. A., Flocke, F.
31 M., and Seinfeld, J. H.: Concentrations and sources of organic carbon aerosols in the free

1 troposphere over North America, *J. Geophys. Res.*, 111, D23S47,
2 doi:10.1029/2006JD007705, 2006.

3 Heald, C. L., J. L. Collett Jr., Lee, T., Benedict, K. B., Schwandner, F. M., Li, Y., Clarisse, L.,
4 Hurtmans, D. R., Van Damme, M., Clerbaux, C., Coheur, P.-F., Philip, S., Martin, R. V., and
5 Pye, H. O. T.: Atmospheric ammonia and particulate inorganic nitrogen over the United
6 States, *Atmos. Chem. Phys.*, 12, 10295-10312, doi:10.5194/acp-12-10295-2012, 2012.

7 Highwood, E. J., Haywood, J. M., Coe, H., Cook, J., Osborne, S., Williams, P., Crosier, J.,
8 Bower, K., Formenti, P., McQuaid, J., Brooks, B., Thomas, G., Grainger, R., Barnaba, F.,
9 Gobbi, G. P., de Leeuw, G., and Hopkins, J.: Aerosol Direct Radiative Impact Experiment
10 (ADRIEX): overview. *Q. J. R. Meteorol. Soc.*, 133, 3-15, 2007.

11 Hodzic, A., Chepfer, H., Vautard, R., Chazette, P., Beekmann, M., Bessagnet, B., Chatenet,
12 B., Cuesta, J., Drobinski, P., Goloub, P., Haeffelin, M., and Morille, Y.: Comparison of
13 aerosol chemistry transport model simulations with lidar and Sun photometer observations at
14 a site near Paris. *J. Geophys. Res.*, 109, D23201, doi:10.1029/2004JD004735, 2004.

15 Hodzic, A., Bessagnet, B., and Vautard, R.: A model evaluation of coarse-mode nitrate
16 heterogeneous formation on dust particles. *Atmos. Environ.*, 40, 4158-4171, 2006.

17 Hodzic, A., Jimenez, J. L., Madronich, S., Aiken, A. C., Bessagnet, B., Curci, G., Fast, J.,
18 Lamarque, J.-F., Onasch, T. B., Roux, G., Schauer, J. J., Stone, E. A., and Ulbrich, I. M.:
19 Modeling organic aerosols during MILAGRO: importance of biogenic secondary organic
20 aerosols, *Atmos. Chem. Phys.*, 9, 6949-6981, doi:10.5194/acp-9-6949-2009, 2009.

21 Hu, X.-M., Klein, P. M., Xue, M., Zhang, F., Doughty, D. C., Forkel, R., Joseph, E., and
22 Fuentes, J. D.: Impact of the vertical mixing induced by low-level jets on boundary layer
23 ozone concentration. *Atmos. Environ.*, 70, 123-130, 2013.

24 Iacono, M. J., Delamere, J. S., Mlawer, E. J., Shephard, M. W., Clough, S. A., and Collins,
25 W. D.: Radiative forcing by long-lived greenhouse gases: Calculations with the AER radiative
26 transfer models, *J. Geophys. Res.*, 113, D13103, doi:10.1029/2008JD009944, 2008.

27 Im, U., Bianconi, R., Solazzo, E., Kioutsioukis, I., Badia, A., Balzarini, A., Baro, R., Bellasio,
28 R., Brunner, D., Chemel, C., Curci, G., Flemming, J., Forkel, R., Giordano, L., Jimenez-
29 Guerrero, P., Hirtl, M., Hodzic, A., Honzak, L., Jorba, O., Knote, C., Kuenen, J. J. P., Makar,
30 P. A., Manders-Groot, A., Neal, L., Perez, J. L., Pirovano, G., Pouliot, G., San Jose, R.,
31 Savage, N., Schroder, W., Sokhi, R. S., Syrakov, D., Torian, A., Tuccella, P., Werhahn, J.,

1 Wolke, R., Yahya, K., Zabkar, R., Zhang, Y., Zhang, J., Hogrefe, C., Galmarini, S.:
2 Evaluation of operational online-coupled regional air quality models over Europe and North
3 America in the context of AQMEII phase 2. Part I: Ozone. *Atmos. Environ.*, doi:
4 10.1016/j.atmosenv.2014.09.042, 2014.

5 Im, U., Bianconi, R., Solazzo, E., Kioutsioukis, I., Badia, A., Balzarini, A., Baro, R., Bellasio,
6 R., Brunner, D., Chemel, C., Curci, G., Denier van der Gon, H., Flemming, J., Forkel, R.,
7 Giordano, L., Jimenez-Guerrero, P., Hirtl, M., Hodzic, A., Honzak, L., Jorba, O., Knote, C.,
8 Makar, P. A., Manders-Groot, A., Neal, L., Perez, J. L., Pirovano, G., Pouliot, G., San Jose,
9 R., Savage, N., Schroder, W., Sokhi, R. S., Syrakov, D., Torian, A., Tuccella, P., Wang, K.,
10 Werhahn, J., Wolke, R., Zabkar, R., Zhang, Y., Zhang, J., Hogrefe, C., Galmarini, S.:
11 Evaluation of operational online-coupled regional air quality models over Europe and North
12 America in the context of AQMEII phase 2. Part II: Particulate Matter. *Atmos. Environ.*, doi:
13 10.1016/j.atmosenv.2014.08.072, 2014.

14 Jenkin, M. E., and Clemitshaw, K. C.: Ozone and other photochemical pollutants: chemical
15 processes governing their formation in the planetary boundary layer. *Atmos. Environ.*, 34,
16 2499-2527, 2000.

17 Johnson, B. T., Shine, K. P., and Forster, P. M.: The semi-direct aerosol effect: Impact of
18 absorbing aerosols on marine stratocumulus. *Q. J. R. Meteorol. Soc.*, 130, 1407-1422, 2004.

19 Kuenen, J. J. P., Visschedijk, A. J. H., Jozwicka, M., and Denier van der Gon, H. A. C.: TNO-
20 MACC_II emission inventory: a multi-year (2003–2009) consistent high-resolution European
21 emission inventory for air quality modelling, *Atmos. Chem. Phys. Discuss.*, 14, 5837-5869,
22 doi:10.5194/acpd-14-5837-2014, 2014.

23 Landi, T. C., Curci, G., Carbone, C., Menut, L., Bessagnet, B., Giulianelli, L., Paglione, M.,
24 Facchini, M. C.: Simulation of size-segregated aerosol chemical composition over Northern
25 Italy in clear sky and wind calm conditions. *Atmos. Res.*, 125-126, 1-11,
26 <http://dx.doi.org/10.1016/j.atmosres.2013.01.009>, 2013.

27 Lee, T., Yu, X.-Y., Ayres, B., Kreidenweis, S. M., Malm, W. C., Collet Jr., J. L.:
28 Observations of fine and coarse particle nitrate at several rural locations in the United States,
29 *Atmos. Environ.*, 42, 2720–2732, doi:10.1016/j.atmosenv.2007.05.016, 2008.

30 Lohmann, U. and Feichter, J.: Global indirect aerosol effects: a review, *Atmos. Chem. Phys.*,
31 5, 715-737, doi:10.5194/acp-5-715-2005, 2005.

1 Lonati, G., Giugliano, M., Butelli, P., Romele, L., and Tardivo, R.: Major chemical
2 components of PM_{2.5} in Milan (Italy). *Atmos. Environ.*, 39, 1925-1934, 2005.

3 Lonati, G., Crippa, M., Gianelle, V., and Van Dingenen, R.: Daily patterns of the multi-modal
4 structure of the particle number size distribution in Milan, Italy. *Atmos. Environ.*, 45, 2434-
5 2442, 2011.

6 Maletto, A., McKendry, I. G., and Strawbridge, K. B.: Profiles of particulate matter size
7 distributions using a balloon-borne lightweight aerosol spectrometer in the planetary
8 boundary layer, *Atmos. Environ.*, 37, 661-670, 2003.

9 Marcazzan, G. M., Vaccaro, S., Valli, G., and Vecchi, R.: Characterization of PM₁₀ and PM_{2.5}
10 particulate matter in the ambient air of Milan (Italy). *Atmos. Environ.*, 35, 4639-4650, 2001.

11 Martilli, A., Neftel, A. Favaro, G., Kirchner, F., Sillman, S., and Clappier, A.: Simulation of
12 the ozone formation in the northern part of the Po Valley. *J. Geophys. Res.*, 107, D22, 8195,
13 doi:10.1029/2001JD000534, 2002.

14 Matta, E., Facchini, M. C., Decesari, S., Mircea, M., Cavalli, F., Fuzzi, S., Putaud, J.-P., and
15 Dell'Acqua, A.: Mass closure on the chemical species in size-segregated atmospheric aerosol
16 collected in an urban area of the Po Valley, Italy, *Atmos. Chem. Phys.*, 3, 623-637,
17 doi:10.5194/acp-3-623-2003, 2003.

18 Mavroidis, I., and Ilia, M.: Trends of NO_x, NO₂ and O₃ concentrations at three different types
19 of air quality monitoring stations in Athens, Greece. *Atmos. Environ.*, 63, 135-147, 2012.

20 McKeen, S. A., Wotawa, G., Parrish, D. D., Hollaway, J. S., Buhr, M. P., Hubler, G.,
21 Fehesenfeld, F. C., and Meagher, J. F.: Ozone production from Canadian wildfires during
22 June and July 1995, *J. Geophys. Res.*, 107(D14), 4192, ACH 7-1–ACH 7-25,
23 doi:10.1029/2001JD000697, 2002.

24 Misenis, C., and Zhang, Y. : An examination of sensitivity of WRF/Chem predictions to
25 physical parameterizations, horizontal grid spacing, and nesting options, *Atmos. Res.*, 97,
26 315-334, 2010.

27 Morgan, W. T., Allan, J. D., Bower, K. N., Capes, G., Crosier, J., Williams, P. I., and Coe, H.:
28 Vertical distribution of sub-micron aerosol chemical composition from North-Western Europe
29 and the North-East Atlantic, *Atmos. Chem. Phys.*, 9, 5389-5401, doi:10.5194/acp-9-5389-
30 2009, 2009.

1 Morino, Y., Kondo, Y., Takegawa, N., Miyazaki, Y., Kita, K., Komazaki, Y., Fukuda, M.,
2 Miyakawa, T., Moteki, N., and Worsnop, D. R.: Partitioning of HNO₃ and particulate nitrate
3 over Tokyo: Effect of vertical mixing, *J. Geophys. Res.*, 111, D15215,
4 doi:10.1029/2005JD006887, 2006.

5 Morrison, H., Thompson, G., and Tatarskii, V.: Impact of cloud microphysics on the
6 development of trailing stratiform precipitation in a simulated squall line: comparison of one-
7 and two-moment scheme, *Mon. Weather Rev.*, 137, 991-1007, doi:10.1175/2008mwr2556.1,
8 2009.

9 Nakanishi, M., and Niino, H.: An improved Mellor-Yamada Level-3 Model: Its numerical
10 stability and application to a regional prediction of advection fog, *Boundary Layer Meteorol.*,
11 119, 397–407, doi:10.1007/s10546-005-9030-8, 2006.

12 Neuman, J. A., Nowak, J. B., Brock, C. A., Trainer, M., Fehsenfeld, F. C., Holloway, J. S.,
13 Hubler, G., Hudson, P. K., Murphy, D. M., Nicks Jr., D. K., Orsini, D., Parrish, D. D.,
14 Ryerson, T. B., Sueper, D. T., Sullivan, A., and Weber, R.: Variability in ammonium nitrate
15 formation and nitric acid depletion with altitude and location over California, *J. Geophys.*
16 *Res.*, 108, D17, 4557, doi:10.1029/2003JD003616, 2003.

17 Novakov, T., Hegg, D. A., and Hobbs, P. V.: Airborne measurements of carbonaceous
18 aerosols on the East Coast of the United States, *J. Geophys. Res.*, 102, D25, 30023-30030,
19 doi: 10.1029/97JD02793, 1997.

20 O’Dowd, C. D., and Smith, M. H.: The vertical structure of aerosol and its relationship to
21 boundary-layer thermodynamics over the rural UK. *Q. J. R. Meteorol. Soc.*, 122, 1799-1814,
22 1996.

23 Oberdorster, G.: Pulmonary effects of inhaled ultrafine particles. *Int. Arch. Occup. Environ.*
24 *Health*, 74, 1-8, 2001.

25 Ordonez, C., Richter, A., Steinbacher, M., Zellweger, C., Nuss, H., Burrows, J. P., and Prévot,
26 A. S. H.: Comparison of 7 years of satellite-borne and ground-based tropospheric NO₂
27 measurements around Milan, Italy. *J. Geophys. Res.*, 111, D05310,
28 doi:10.1029/2005JD006305, 2006.

29 Ouwersloot, H. G., Vilà-Guerau de Arellano, J., Nölscher, A. C., Krol, M. C., Ganzeveld, L.
30 N., Breitenberger, C., Mammarella, I., Williams, J., and Lelieveld, J.: Characterization of a

1 boreal convective boundary layer and its impact on atmospheric chemistry during HUMPPA-
2 COPEC-2010, *Atmos. Chem. Phys.*, 12, 9335-9353, doi:10.5194/acp-12-9335-2012, 2012.

3 Perrone, M. G., Gualtieri, M., Ferrero, L., Lo Porto, C., Udisti, R., Bolzacchini, E., and
4 Camatini, M.: Seasonal variations in chemical composition and in vitro biological effects of
5 fine PM from Milan. *Chemosphere*, 78, 1368-1377, 2010.

6 Perrone, M. G., Larsen, B. R., Ferrero, L., Sangiorgi, G., De Gennaro, G., Udisti, R.,
7 Zangrando, R., Gambaro, A., Bolzacchini, E.: Sources of high PM_{2.5} concentrations in Milan,
8 Northern Italy: Molecular marker data and CMB modelling. *Sci. Total Environ.*, 414, 343-
9 355, 2012.

10 Perrone, M. G., Gualtieri, M., Consonni, V., Ferrero, L., Sangiorgi, G., Longhin, E., Ballabio,
11 D., Bolzacchini, E., and Camatini, M.: Particle size, chemical composition, seasons of the
12 year and urban, rural or remote site origins as determinants of biological effects of particulate
13 matter on pulmonary cells. *Environ. Pollut.*, 176, 215-227, 2013.

14 Poschl, U.: Atmospheric aerosols: Composition, transformation, climate and health effects.
15 *Angew. Chem. Int. Ed.*, 44, 7520-7540, 2005.

16 Prévot, A. S. H., Staehelin, J., Kok, G. L., Schillawski, R. D., Neiningner, B., Staffelbach, T.,
17 Neftel, A., Wernli, H., and Dommen, J.: The Milan photooxidant plume. *J. Geophys. Res.*,
18 102, D19, 23375-23388, 1997.

19 Putaud, J.-P., Van Dingenen, R., and Raes, F.: Submicron aerosol mass balance at urban and
20 semirural sites in the Milan area (Italy). *J. Geophys. Res.*, 107, D22, 8198,
21 doi:10.1029/2000JD000111, 2002.

22 Putaud, J.-P., Van Dingenen, R., Alastuey, A., Bauer, H., Birmili, W., Cyrys, J., Flentje, H.,
23 Fuzzi, S., Gehrig, R., Hansson, H. C., Harrison, R. M., Herrmann, H., Hitzenberger, R.,
24 Hüglin, C., Jones, A. M., Kasper-Giebl, A., Kiss, G., Kousam, A., Kuhlbusch, T. A. J.,
25 Löschau, G., Maenhaut, W., Molnar, A., Moreno, T., Pekkanen, J., Perrino, C., Pitz, M.,
26 Puxbaum, H., Querol, X., Rodriguez, S., Salma, I., Schwarz, J., Smolik, J., Schneider, J.,
27 Spindler, G., ten Brink, H., Tursic, J., Viana, M., Wiedensohler, A., and Raes F.: A European
28 aerosol phenomenology – 3: Physical and chemical characteristics of particulate matter from
29 60 rural, urban, and kerbside sites across Europe, *Atmos. Environ.*, 44, 1308-1320, 2010.

1 Raes, F., Van Dingenen, R., Vignati, E., Wilson, J., Putaud, J.-P., Seinfeld, J. H., and Adams,
2 P.: Formation and cycling of aerosols in the global troposphere. *Atmos. Environ.*, 34, 4215-
3 4240, 2000.

4 Saarikoski, S., Carbone, S., Decesari, S., Giulianelli, L., Angelini, F., Canagaratna, M., Ng,
5 N. L., Trimborn, A., Facchini, M. C., Fuzzi, S., Hillamo, R., and Worsnop, D.: Chemical
6 characterization of springtime submicrometer aerosol in Po Valley, Italy, *Atmos. Chem.*
7 *Phys.*, 12, 8401-8421, doi:10.5194/acp-12-8401-2012, 2012.

8 Saxena, P., Hudischewskij, A. B., Seigneur, C., and Seinfeld, J. H.: A comparative study of
9 equilibrium approaches to the chemical characterization of secondary aerosols, *Atmos.*
10 *Environ.*, 20, 1471–1483, 1986.

11 Schurmann, G. J., Algieri, A., Hedgecock, I. M., Manna, G., Pirrone, N., and Sprovieri, F.:
12 Modelling local and synoptic scale influences on ozone concentrations in a topographically
13 complex region of Southern Italy, *Atmos. Environ.*, 43, 4424-4434, 2009.

14 Seinfeld, J. H., and Pandis, S. N.: *Atmospheric chemistry and physics: From air pollution to*
15 *climate change*, Second Edition. Wiley-Interscience editions, pp. 1203, 2006.

16 Silibello, C., Calori, G., Brusasca, G., Giudici, A., Angelino, E., Fossati, G., Peroni, E., and
17 Buganza, E.: Modelling of PM₁₀ concentrations over Milano urban area using two aerosol
18 modules. *Environ. Modell. Softw.*, 23, 333-343, 2008.

19 Squizzato, S., Masiol, M., Brunelli, A., Pistollato, S., Tarabotti, E., Rampazzo, G., and
20 Pavoni, B.: Factors determining the formation of secondary inorganic aerosol: a case study in
21 the Po Valley (Italy), *Atmos. Chem. Phys.*, 13, 1927-1939, doi:10.5194/acp-13-1927-2013,
22 2013.

23 Stockwell, W. R., Kirchner, F., Kuln, M., and Seefeld, S.: A new mechanism for regional
24 atmospheric chemistry modelling, *J. Geophys. Res.*, 102(D22), 25, 847-25, 879,
25 doi:10.1029/97JD00849, 1997.

26 Stull, R. B.: *An introduction to boundary layer meteorology*. Atmospheric Sciences Library,
27 Kluwer Academic Publishers, 666 p., 1988.

28 Tai, A. P. K., Mickley, L. J., and Jacob, D. J.: Correlations between fine particulate matter
29 (PM_{2.5}) and meteorological variables in the United States: Implications for the sensitivity of
30 PM_{2.5} to climate change. *Atmos. Environ.*, 44, 3976-3984, 2010.

1 Tuccella, P., Curci, G., Visconti, G., Bessagnet, B., Menut, L., Park, R. J.: Modelling of gas
2 and aerosol with WRF/Chem over Europe: evaluation and sensitivity study. *J. Geophys. Res.*,
3 117, D03303, doi:10.1029/2011JD016302, 2012.

4 Tuccella, P., Curci, G., Grell, G. A., Visconti, G., Crumeyrolle, S., Schwarzenboeck, A., and
5 Mensah, A. A.: A new chemistry option in WRF/Chem v. 3.4 for the simulation of direct and
6 indirect aerosol effects using VBS: evaluation against IMPACT-EUCAARI data, *Geosci.*
7 *Model Dev. Discuss.*, 8, 791-853, doi:10.5194/gmdd-8-791-2015, 2015.

8 van Donkelaar, A., Martin, R. V., Brauer, M., Kahn, R., Levy, R., Verduzco, C., and
9 Villeneuve, P. J.: Global estimates of ambient fine particulate matter concentrations from
10 satellite-based Aerosol Optical Depth: Development and application. *Environ. Health Persp.*,
11 118, 847-855, 2010.

12 van Stratum, B. J. H., Vilà-Guerau de Arellano, J., Ouwersloot, H. G., van den Dries, K.,
13 van Laar, T. W., Martinez, M., Lelieveld, J., Diesch, J.-M., Drewnick, F., Fischer, H.,
14 Hosaynali Beygi, Z., Harder, H., Regelin, E., Sinha, V., Adame, J. A., Sörgel, M., Sander, R.,
15 Bozem, H., Song, W., Williams, J., and Yassaa, N.: Case study of the diurnal variability of
16 chemically active species with respect to boundary layer dynamics during DOMINO, *Atmos.*
17 *Chem. Phys.*, 12, 5329-5341, doi:10.5194/acp-12-5329-2012, 2012.

18 Walcek, C. J., and Taylor, G. R.: A Theoretical Method for Computing Vertical Distributions
19 of Acidity and Sulfate Production within Cumulus Clouds. *J. Atmos. Sci.*, 43, 339–355,
20 1986.

21 Wesely, M. L.: Parameterization of surface resistance to gaseous dry deposition in regional-
22 scale numerical models, *Atmos. Environ.*, 23, 1293–1304, doi:10.1016/0004-6981(89)90153-
23 4, 1989.

24 Whiteman, C. D.: Observations of thermally developed wind systems in mountainous terrain.
25 Chapter 2 in *Atmospheric Processes Over Complex Terrain* (W. Blumen Ed.), *Meteorological*
26 *Monographs*, 23, 5-42, 1990.

27 Wild, O., X. Zhu, and Prather, M. J.: Fast-J: Accurate simulation of in- and below cloud
28 photolysis in tropospheric chemical models, *J. Atmos. Chem.*, 37, 245–282,
29 doi:10.1023/A:1006415919030, 2000.

30 Wonaschuetz, A., Sorooshian, A., Ervens, B., Chuang, P. Y., Feingold, G., Murphy, S. M., de
31 Gouw, J., Warneke, C., and Jonsson, H. H.: Aerosol and gas re-distribution by shallow

1 cumulus clouds: An investigation using airborne measurements. *J. Geophys. Res.*, 117,
2 D17202, doi:10.1029/2012JD018089, 2012.

3 Wong, D. N., Barth, M. Skamarock, W., Grell, G., Worden, J.: A Budget of the Summertime
4 Ozone Anomaly Above Southern United States using WRF-Chem. AGU Fall Meeting, San
5 Francisco, CA, USA, 14-18 December, 2009.

6 Yu, H., Kaufman, Y. J., Chin, M., Feingold, G., Remer, L. A., Anderson, T. L., Balkanski, Y.,
7 Bellouin, N., Boucher, O., Christopher, S., DeCola, P., Kahn, R., Koch, D., Loeb, N., Reddy,
8 M. S., Schulz, M., Takemura, T., and Zhou, M.: A review of measurement-based assessments
9 of the aerosol direct radiative effect and forcing, *Atmos. Chem. Phys.*, 6, 613-666,
10 doi:10.5194/acp-6-613-2006, 2006.

11 Zhang, Q., Jimenez, J. L., Canagaratna, M. R., Allan, J. D., Coe, H., Ulbrich, I., Alfarra, M.
12 R., Takami, A., Middlebrook, A. M., Sun, Y. L., Dzepina, K., Dunlea, E., Docherty, K.,
13 DeCarlo, P. F., Salcedo, D., Onasch, T., Jayne, J. T., Miyoshi, T., Shimono, A., Hatakeyama,
14 S., Takegawa, N., Kondo, Y., Schneider, J., Drewnick, F., Borrmann, S., Weimer, S.,
15 Demerjian, K., Williams, P., Bower, K., Bahreini, K., Cottrell, L., Griffin, R. J., Rautiainen,
16 J., Sun, J. Y., Zhang, Y. M., and Worsnop, D. R.: Ubiquity and dominance of oxygenated
17 species in organic aerosols in anthropogenically-influenced Northern Hemisphere
18 midlatitudes. *Geophys. Res. Lett.*, 34, L13801, doi:10.1029/2007GL029979, 2007.

19 Zhang, Y., Wen, X.-Y., Wang, K., Vijayaraghavan, K., and Jacobson, M. Z.: Probing into
20 regional O₃ and particulate matter pollution in the United States: 2. An examination of
21 formation mechanisms through a process analysis technique and sensitivity study. *J. Geophys.*
22 *Res.*, 114, D22305, doi:10.1029/2009JD011900, 2009.

23 Zhang, Y., Liu, P., Liu, X.-H., Jacobson, M. Z., McMurry, P. H., Yu, F., Yu, S., and Schere,
24 K. L.: A comparative study of nucleation parameterizations: 2. Three-dimensional model
25 application and evaluation. *J. Geophys. Res.*, 115, D20213, doi:10.1029/2010JD014151,
26 2010.

27

1 Table 1. Main physical and chemical parameterizations used in WRF/Chem simulations.

Process	Scheme
Short-wave radiation	RRTM
Long-wave radiation	RRTM
Surface Layer	Monin-Obukov
Boundary Layer	MYNN
Land surface model	Noah LSM
Cumulus convection	Grell scheme G3
Cloud microphysics	Morrison
Gas-phase mechanism	RACM-ESRL
Aerosol mechanism	MADE/SOA-VBS
Photolysis	Fast-J
Cloud chemistry and wet deposition	On
Biogenic emissions	MEGAN
Direct aerosol effect	On
Indirect aerosol effects	Off

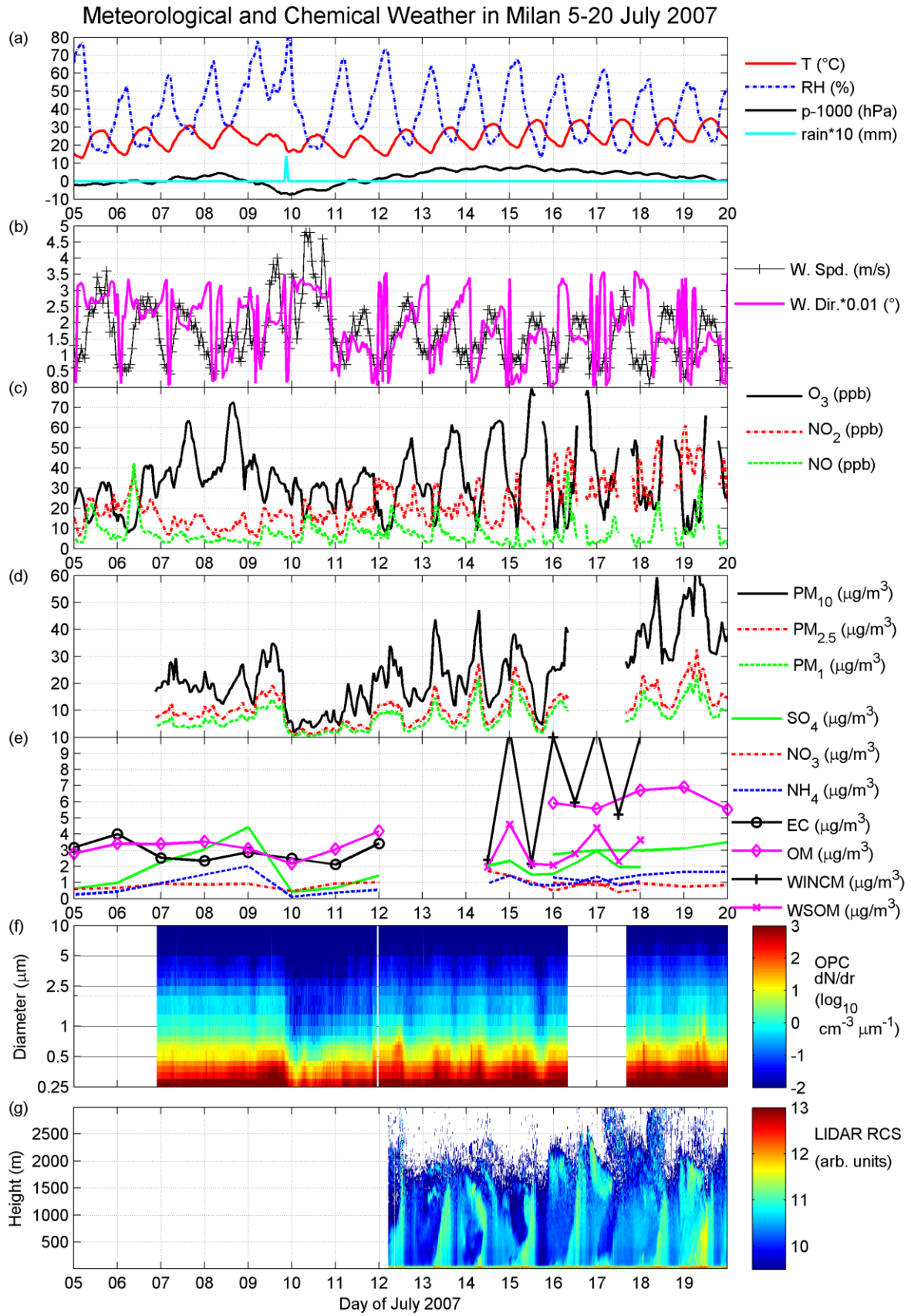
2

3

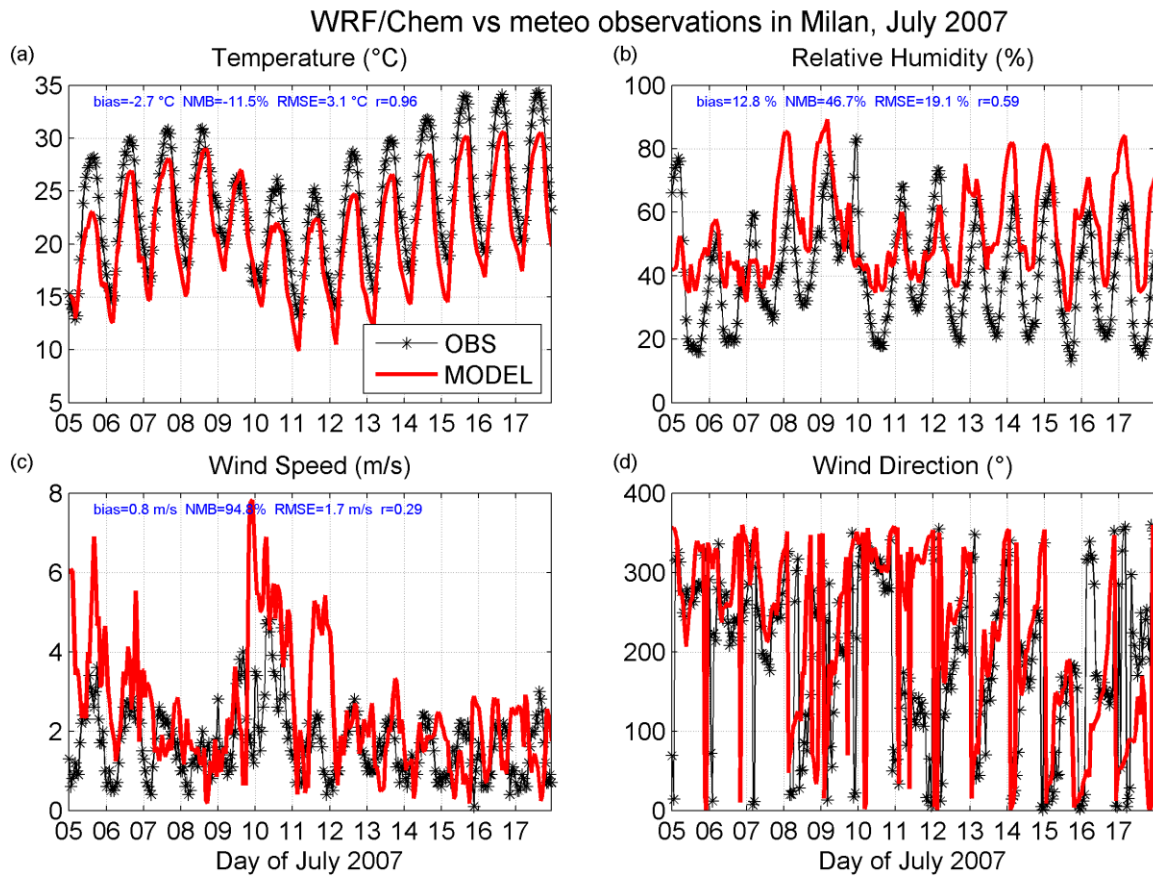
1 Table 2. Description of sensitivity tests with WRF/Chem model.

Label	Description
CTRL	Reference run, see Table 1.
AERO	Aerosol chemical processes switched off
LPBL	Gas and aerosol chemical processes switched off in the Lower half of the PBL
UPBL	Gas and aerosol chemical processes switched off in the Upper half of the PBL
APBL	Gas and aerosol chemical processes switched off Above the PBL

2



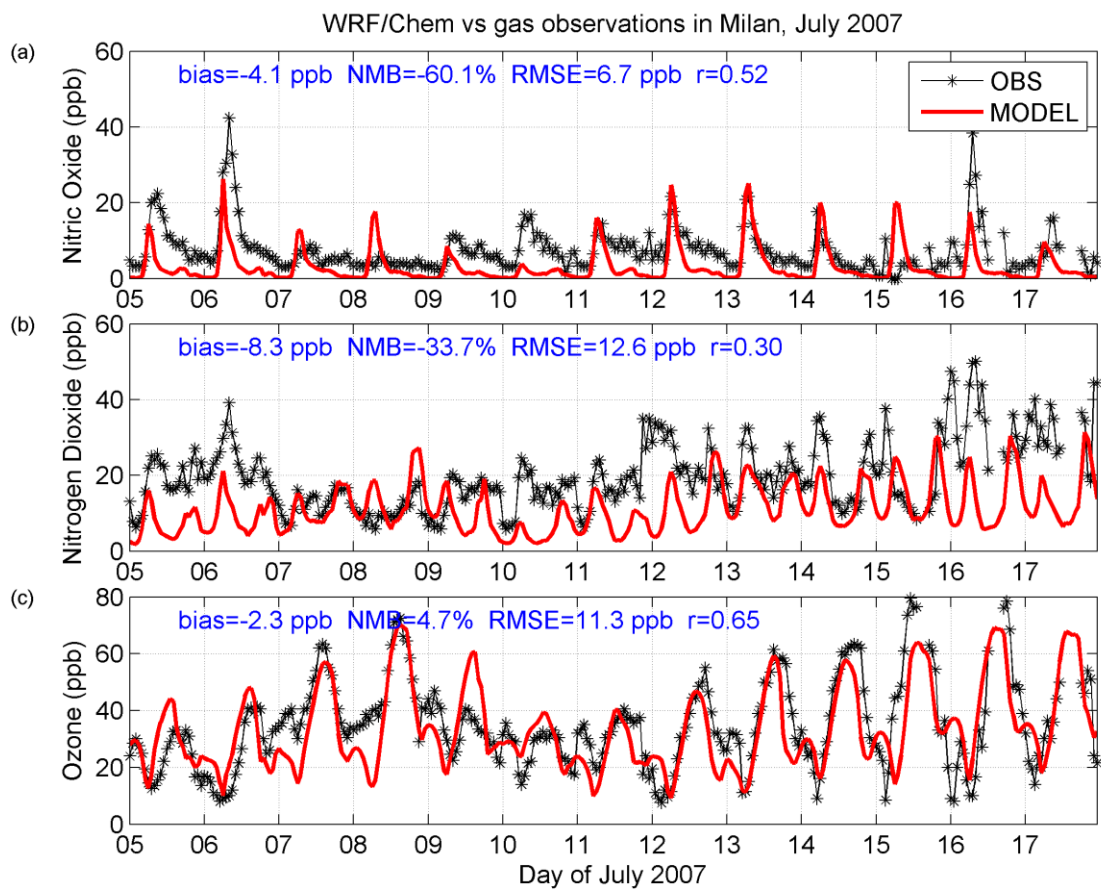
1 Figure 1. Ground-based observations in Milan during July 5-20, 2007. Panel (a) shows hourly
2 measurements of temperature, relative humidity, pressure and precipitation. Pressure is
3 subtracted by 1000 and precipitation is multiplied by 10 in order to fit the same y-axis. (b)
4 Hourly wind speed and wind direction (0° from the North, 90° from the East), the latter
5 divided by 100 to fit the same y-axis. (c) Hourly ozone, nitrogen dioxide and nitrogen oxide.
6 (d) Particulate matter mass. Hourly observations of PM_{10} , $PM_{2.5}$, and PM_1 . (d) Particulate
7 matter composition. Daily data of sulfate, nitrate, ammonium, elemental carbon and organic
8 matter collected during QUITSAT campaign. Night-time (21 to 08 local solar time) and day-
9 time (08 to 21 LST) samples of sulfate, nitrate, ammonium, water-insoluble carbonaceous
10 matter (WINCM) and water-soluble organic matter (WSOM) collected during AeroClouds
11 campaign (July 14-17). (e) Particulate matter number size distribution. Optical particle
12 counter (OPC) hourly average measurements, y-axis denotes the size bin. (f) Particulate
13 matter vertical profile. LIDAR Range Corrected Signal, y-axis denotes the height above
14 ground level.
15



1

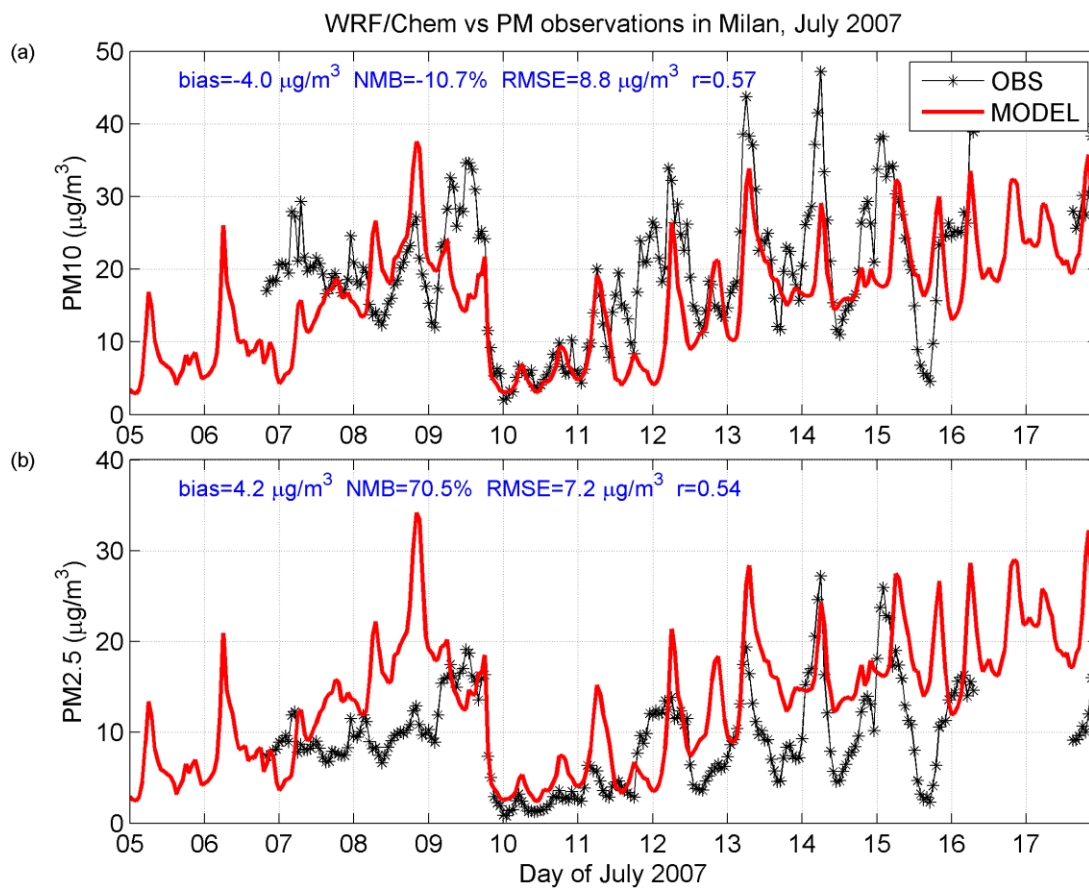
2 Figure 2. Comparison of observed and simulated hourly meteorological variables at ground
 3 level in Milan on July 5-17, 2007. Simulations are carried out with WRF/Chem model and
 4 results are shown for the nested domain over Northern Italy at 10 km horizontal resolution.
 5 Statistical indices shown inset are defined in Appendix A.

6



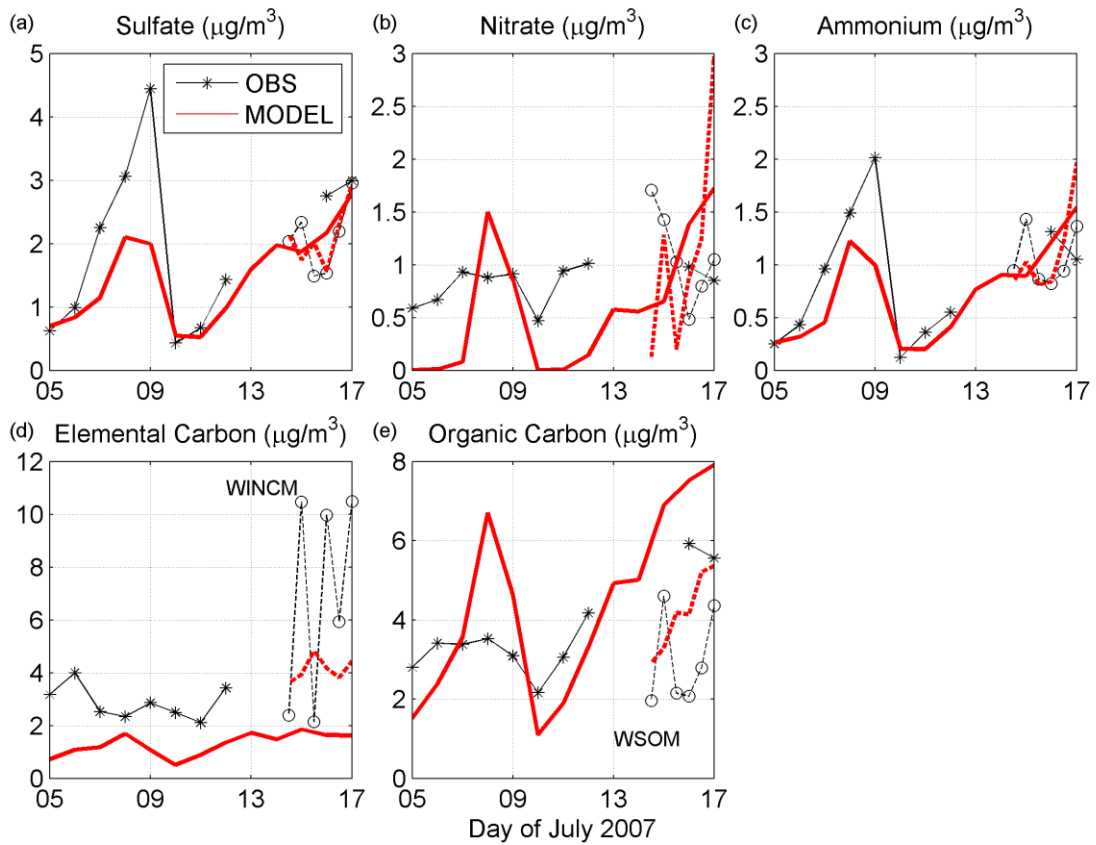
1

2 Figure 3. Same as Figure 2, but for hourly gas-phase variables at ground level in Milan on
 3 July 5-17, 2007. Shown inset are statistical indices defined in Appendix A.



1

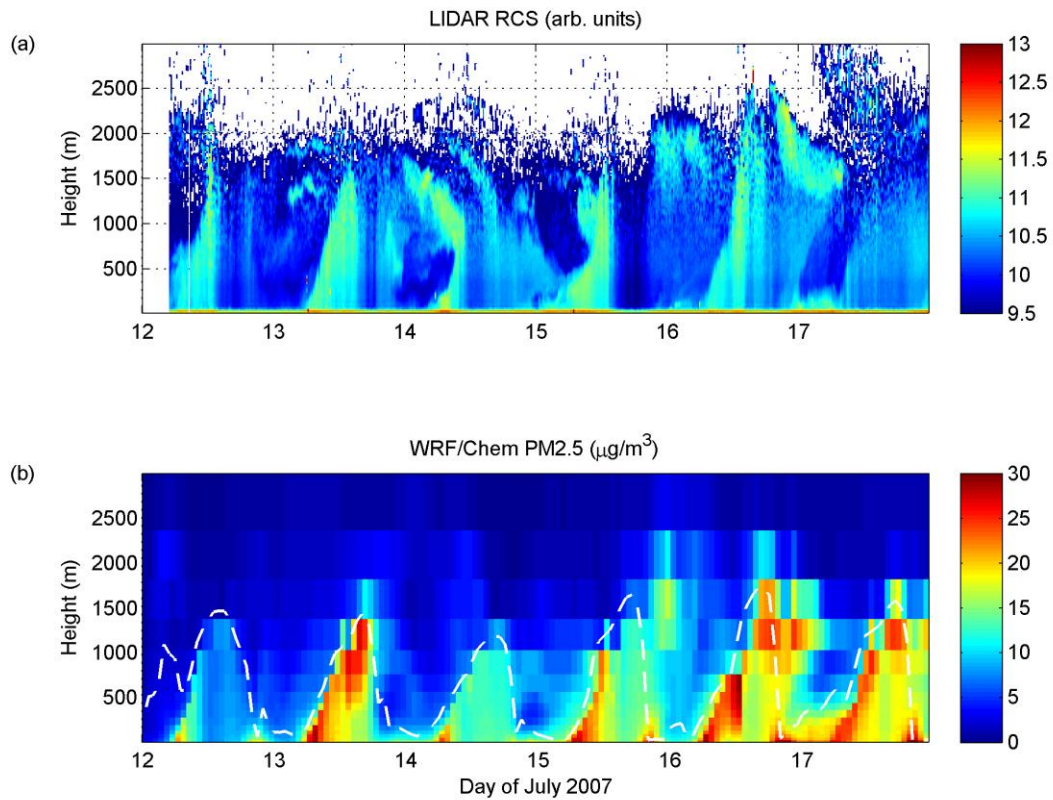
2 Figure 4. Same as Figure 2, but for hourly particulate matter at ground level in Milan on July
 3 5-17, 2007. Shown inset are statistical indices defined in Appendix A.



1

2 Figure 5. Same as Figure 2, for daily (solid lines) and bi-daily (dashed lines) particulate
 3 matter composition at ground level in Milan on July 5-17, 2007. Bi-daily observations
 4 (dashed lines) are available only from July 14 to 17. In panel (d), WINCM is the Water
 5 Insoluble Carbon Mass (EC + mostly primary OC), in panel (e) WSOM is Water Soluble
 6 Organic Mass (mostly secondary organic aerosol, Carbone et al., 2010).

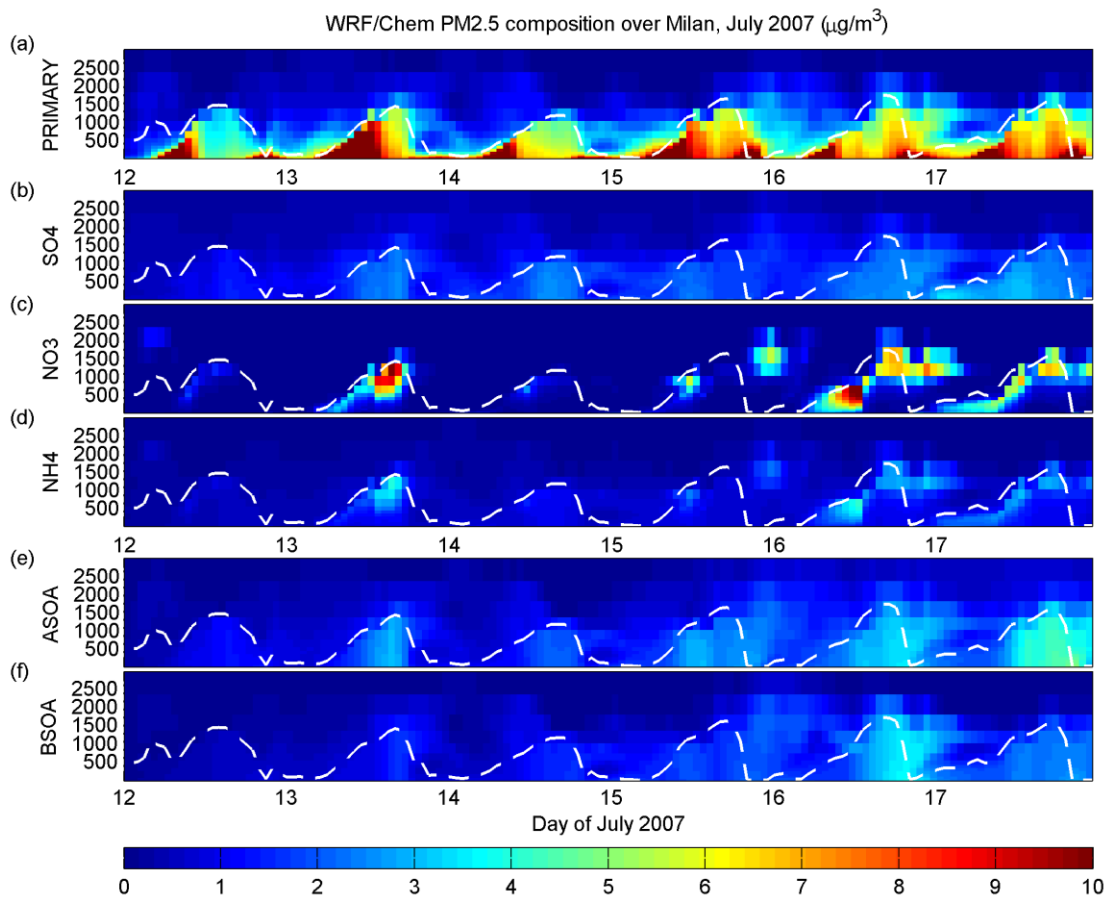
7



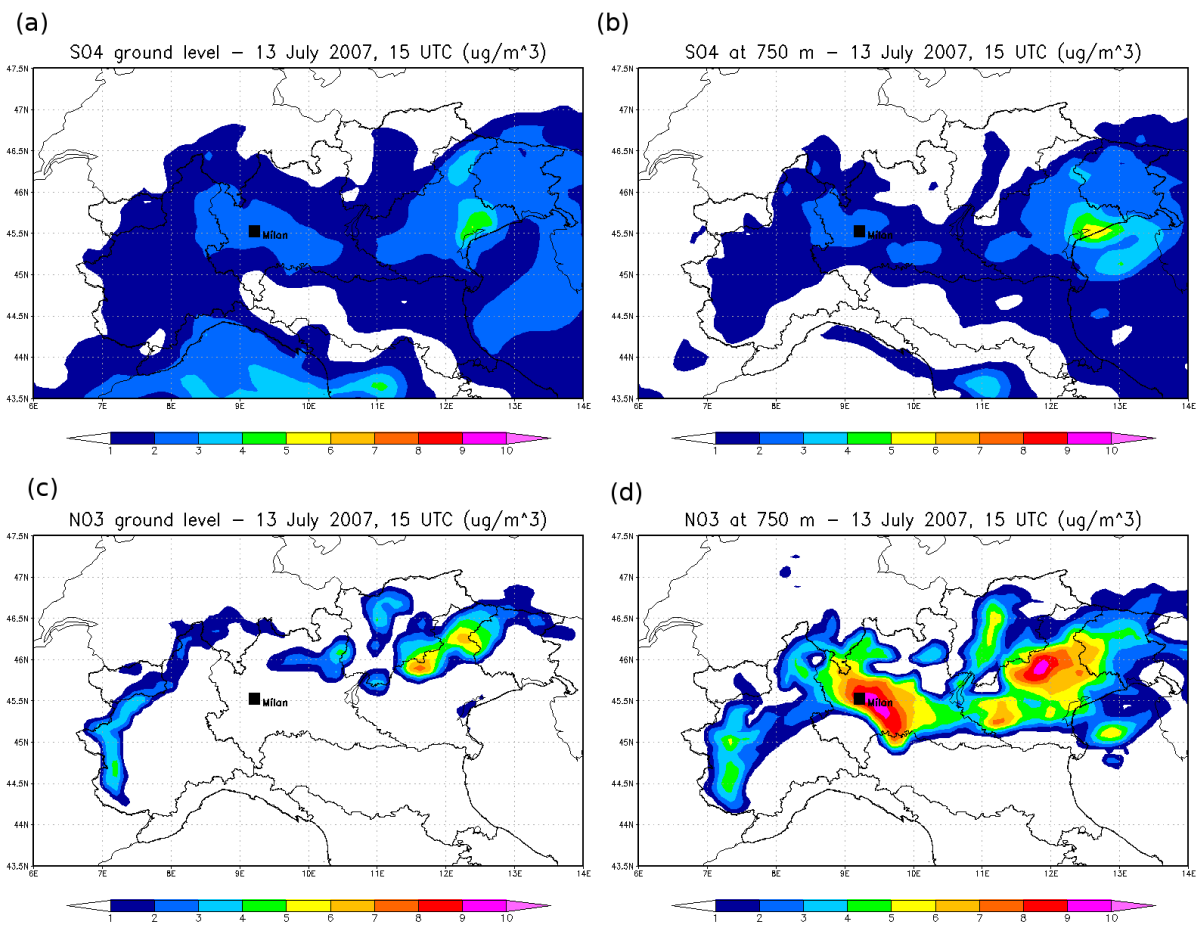
1

2 Figure 6. Qualitative comparison of (a) LIDAR Range Corrected Signal and (b) simulated
 3 PM_{2.5} vertical profile over Milan on July 12-17, 2007. The white dashed line in the bottom
 4 panel denotes the simulated PBL height.

5

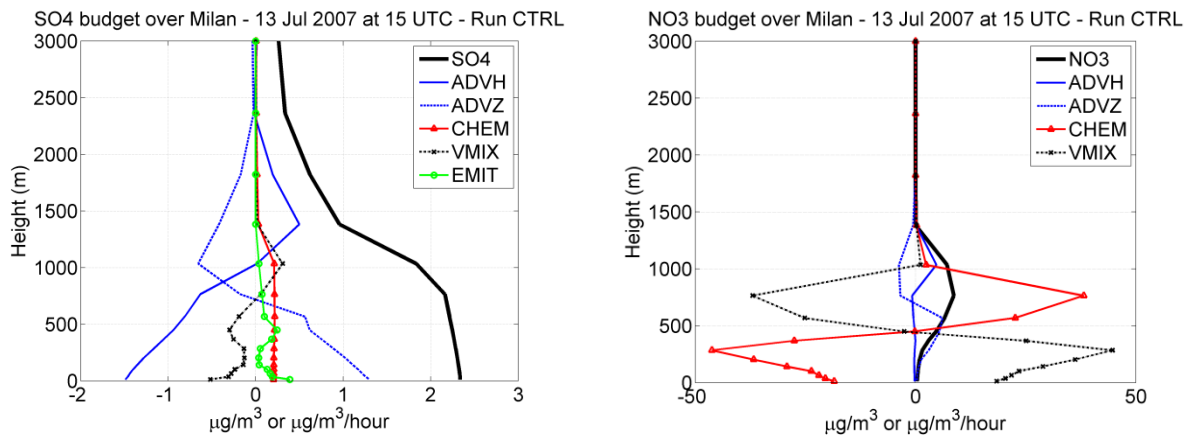


1
2 Figure 7. Simulated composition of PM_{2.5} profile shown in Figure 6. ASOA and BSOA in
3 panels (e) and (f) are anthropogenic and biogenic secondary organic aerosol, respectively.
4



1
2
3
4
5

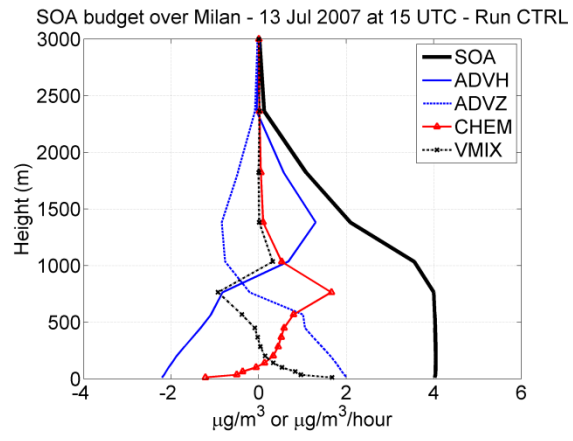
Figure 8. Maps of the concentration of $\text{PM}_{2.5}$ sulfate (a-b) and nitrate (c-d) components simulated at 16 LST of July 13, 2007 over Po Valley. Panels (a-c) are at ground level (the first model level is about 24 m thick), panels (b-d) at approximately 750 m height.



1 Figure 9. Simulated vertical profile of concentration ($\mu\text{g}/\text{m}^3$) and continuity equation terms
 2 ($\mu\text{g}/\text{m}^3/\text{h}$) for particulate sulfate (left) and nitrate (right) at 16 LST of July 13, 2007 over
 3 Milan. Budget terms are: horizontal advection (ADVH), vertical advection (ADVZ),
 4 chemistry (CHEM), turbulent mixing and dry deposition (VMIX), emission (EMIT).

5

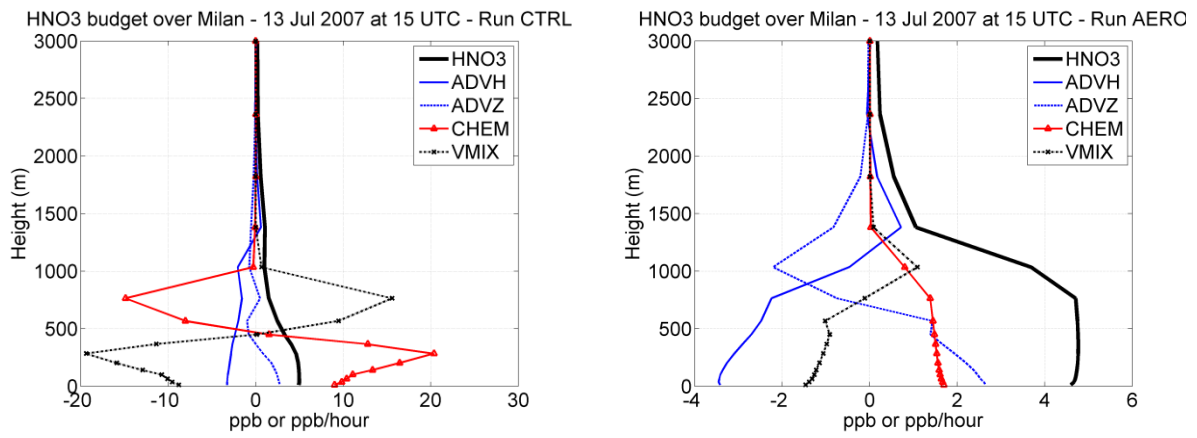
6



1

2 Figure 10. Same as Figure 9, but for Secondary Organic Aerosol (SOA).

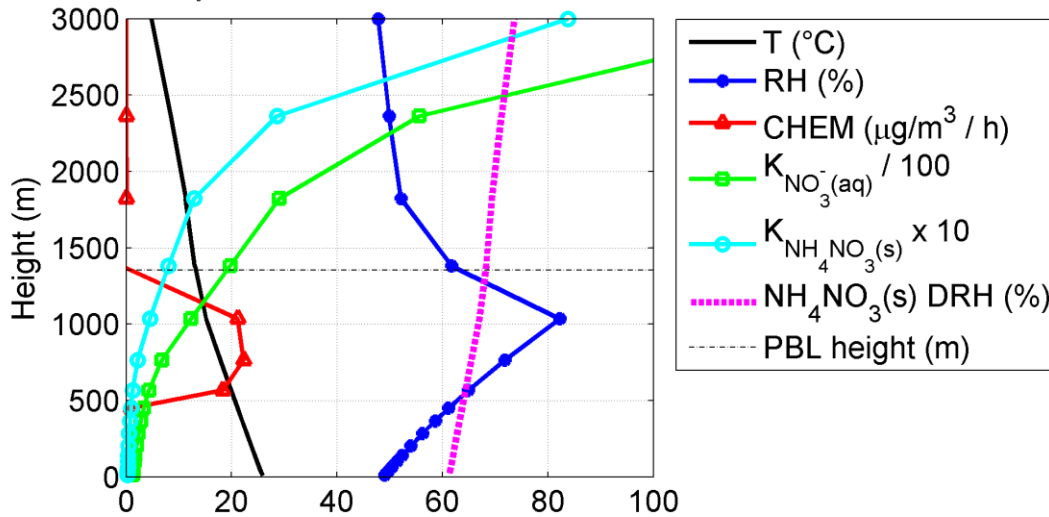
3



1 Figure 11. Same as Figure 9, but for nitric acid (HNO_3) and units in ppb. On the left the
 2 reference simulation (CTRL), on the right a sensitivity simulation with aerosol chemistry
 3 switched off (AERO). Please notice the different abscissa range.

4

Nitrate thermodynamics over Milan - 13 Jul 2007 at 15 UTC

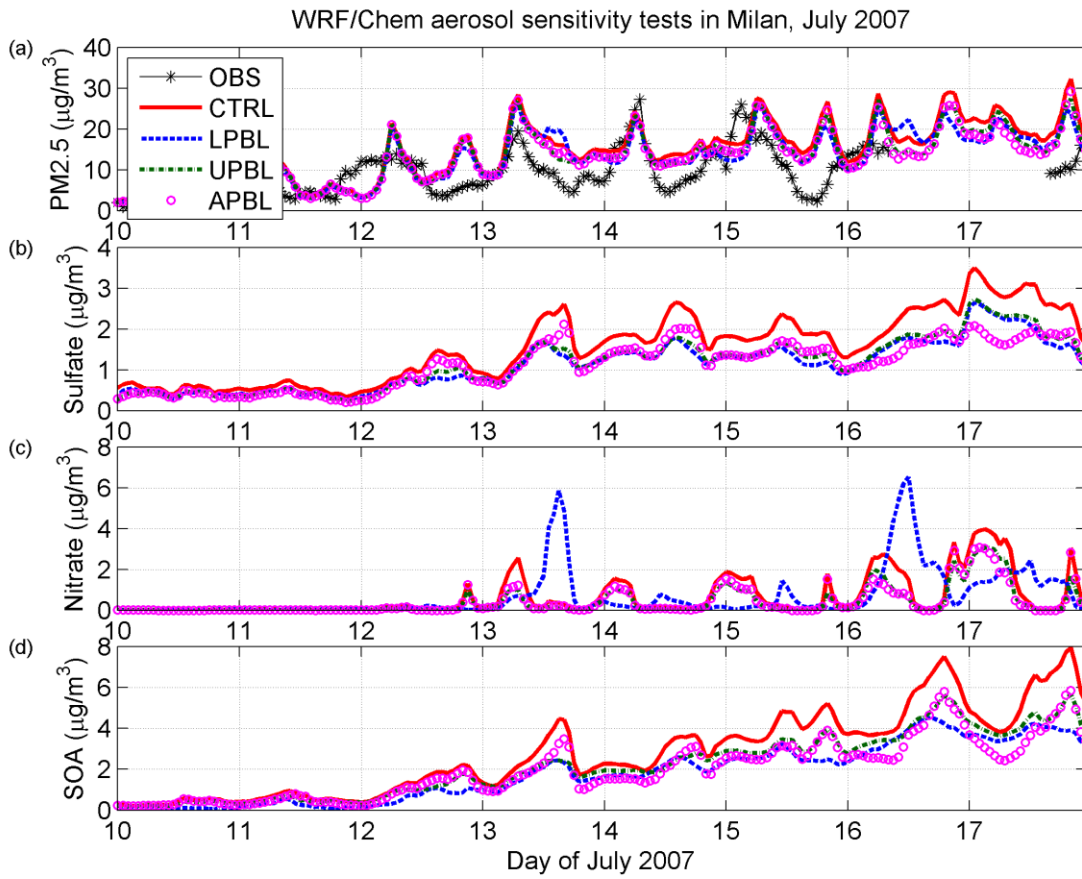


1

2 Figure 12. Simulated vertical profile of relative humidity (blue) and particulate nitrate net
 3 chemical production term (red, triangles) at 16 LST of July 13, 2007 over Milan. Also shown,
 4 vertical profiles of equilibrium constants of aqueous phase nitrate (green, squares) and solid
 5 ammonium nitrate (cyan, circles), and ammonium nitrate deliquescence relative humidity
 6 (magenta, dashed). The height of PBL is denoted by the horizontal black dashed line. Please
 7 note that equilibrium constants are scaled by the constant factors shown inset to fit on the
 8 same abscissa range.

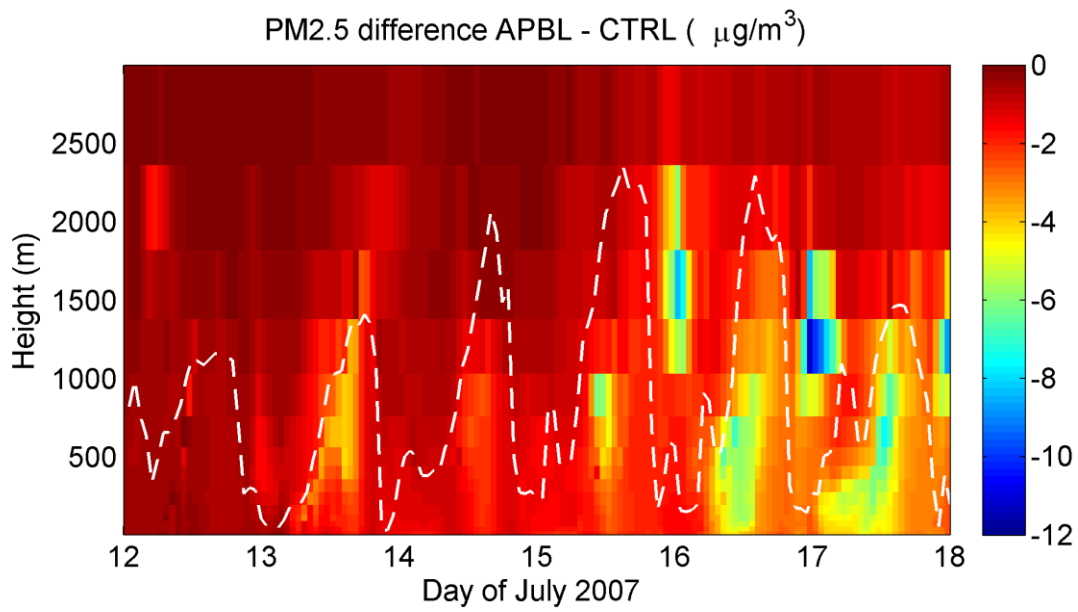
9

10



1
 2 Figure 13. Sensitivity tests on chemical production in different vertical layers (see Table 2 for
 3 explanation of labels), at ground level over Milan on July 10-17, 2007. Hourly observations
 4 (black line-star) are only available for PM_{2.5} (top panel).

5



1

2 Figure 14. Difference of the simulated $\text{PM}_{2.5}$ profile over Milan between APBL and CTRL
 3 runs (see Table 2). Useful to estimate the impact of aerosol residual layer on ground
 4 concentrations, in combination with Figure 6b.

5

6